UNIVERSITY OF CALIFORNIA
RIVERSIDE

An R Shiny App for Integrating Sequencing Datasets in the Analysis of Toxicant Defects Within Osteogenic Differentiation

A Thesis submitted in partial satisfaction
of the requirements for the degree of

Master of Science

in

Cell, Molecular & Developmental Biology

by

Desiree Williams

December 2022

Thesis Committee:
Dr. Nicole I. zur Nieden, Chairperson
Dr. Thomas Girke
Dr. Joshua Morgan

The Thesis of Desiree Williams is approved:

Committee Chairperson

University of California, Riverside

ACKNOWLEDGEMENTS

I would like to acknowledge my professor Nicole zur Nieden who gave me the time and space to discover and learn on my own the skills that helped accomplish this work. Also, a big thank you to Nicole Sparks for her contributions to this work and input that helped make this thesis better. I am also grateful for, and would like to thank my committee members, Thomas Girke and Joshua Morgan for their guidance and patience. Lastly, I am grateful to all my lab members that provided their comments which contributed to this work.

ABSTRACT OF THE THESIS

An R Shiny App for Integrating Sequencing Datasets in the Analysis of Toxicant Defects Within Osteogenic Differentiation

by

Desiree Williams

Master of Science, Cell, Molecular & Developmental Biology
University of California, Riverside, December 2022
Dr. Nicole I. zur Nieden, Chairperson

A class of small, non-coding RNAs, microRNAs (miRNAs), may play a pivotal role in the development of the neural crest (NC)- and mesoderm-derived skeleton. They are involved in a variety of biological processes that contribute to skeletal development, such as, cell migration, Wnt signaling and specification of cellular fate towards osteogenesis. Identifying miRNAs involved with regulating genes that drive the two lineages that give rise to osteoblasts during development can provide distinct gene regulatory mechanisms that give rise to craniofacial deformities. Potential microRNA-to-gene target interaction (MTIs) pairs can then potentially be used as biomarkers for *in utero* diagnostic or treatments for skeletal deformities in the face or limbs. The aim of this study was to develop a set of miRNA biomarkers that correlate with NC and mesoderm cell differentiation into osteoblasts, and to identify miRNAs specific to these pathways. Our study was conducted *in vitro* using human embryonic stem cells (hESCs) that were differentiated into osteoblasts. Toxicants known to repress NC and mesoderm induction were supplied to the *in vitro* cultures and the RNA sequenced to obtain both small RNAs and mRNAs. To facilitate this analysis, an R Shiny web app was developed

to implement the sequencing results of both microRNA and RNA. The app provides tools to separately display and visualize the results of the differential regulation of microRNAs and mRNAs. Gene ontology (GO) analysis revealed that the identified miRNA-target interactions were indeed involved in select GO pathways related to osteogenic, NC and mesoderm differentiation. The app narrowed down significantly correlated MTIs specific to each differentiation lineage. Within the NC lineage miR-30a, miR-148a and miR-195 were correlated with cadherin2 (*CDH2)*, DNA methyltransferase 3 beta (*DNMT3B*) and transcription factor AP-2 alpha (*TFAP2A*), respectively. Within the mesoderm lineage miR-148a, miR-7 and miR-20a were correlated with *DNMT3B*, *JARID2* and *VANGL1*, respectively. In the future, these miRNAs could be further validated as potential biomarkers in the context of neurocristopathies.

Table of Contents

List of Figures

List of Tables

Introduction

Developmental defects such as cleft palate arise from both environmental and genetic factors but are often attributed to misregulation in gene expression. This particular defect forms when the medial nasal processes or the maxillary prominences fail to fuse properly, as a result of improper differentiation of neural crest cells (NCCs). During development the neural crest cells migrate away from the neural tube towards the frontonasal region and undergo identity changes, which are often directed by transcriptional activity. The differentiation of uncommitted cells into a multipotent NCC population is invoked by a complex gene regulatory network (Simões-Costa & Bronner, 2015). One aspect of this network are microRNAs (miRs) that contribute to embryonic development through epigenetic control of genes involved with development (Gebert & MacRae, 2019; Sera & Zur Nieden, 2017; Weiner, 2018). Understanding how miRs contribute to the gene regulatory network (GRN) of NCC differentiation into osteoblasts could be used to develop tools to screen for developing embryos for their risk for neurocristopathies or may be developed as possible targets for treatments. To facilitate the identification of such miRNAs, a web app was designed, to develop a user-friendly analysis interface with which to interrogate microRNA and mRNA next-generation sequencing data sets separately and in combination. In the process, miRNA and mRNA signatures will be developed that characterize each lineage these toxicants affect and identify significantly correlated mRNAs within these lineages. The results from this study may ultimately aid in the identification of potential miR biomarkers.

MicroRNA Biogenesis

MicroRNAs (miRs) are noncoding RNAs first discovered in *Caenorhabditis elegans* (R. C. Lee et al., 1993; Wightman et al., 1993). It was later discovered that they are conserved across a range of animal species (Pasquinelli et al., 2000). These miRs are first transcribed in the nucleus by RNA polymerase II (Y. Lee et al., 2004), mainly from introns and a few exons from protein coding genes (Kim & Kim, 2007), where they are capped at the 5' end (7-methylguanosine) and poly-adenylated at the 3' end. A complex composed of Drosha and DiGeorge Syndrome Critical Region 8 (DGCR8), cleaves the miR into a long system-loop RNA (~70 nucleotides long) called a pre-miRNA. The pre-miRNA is then exported into the cytoplasm by Exportin5 where Dicer cleaves the loop. The now mature miR (average of 22 nt long) complexes with Argonaute (AGO), forming the miRNA-induced silencing complex (miRISC). The passenger strand (strand not loaded into AGO) is unwound and degraded (Ha & Kim, 2014). The miRISC with the guide strand is then directed to a target mRNA for post-transcriptional gene silencing. The 5' binding region of the miR known as a 2-8 nt long seed region binds to the 3'-untranslated region (UTR) of mRNAs normally leading to mRNA degradation and consequent repression of mRNA translation (Setten et al., 2019). Only under special conditions, such as the G0 phase of the cell cycle or interaction with gene promoters, microRNAs were seen to increase or activate gene expression (Broughton et al., 2016; Ramchandran & Chaluvally-Raghavan, 2017; Vasudevan, 2012). Currently, ~2,600 mature microRNAs are annotated in humans and are predicted to target 60% of protein-coding genes (Friedman et al., 2009; Kozomara et al., 2019). miRs are surprisingly stable, detected within many bodily fluids from blood

plasma, semen, saliva, and breast milk (Weber et al., 2010). This makes them attractive in non-invasive screening or as potential targets for treatments.

MicroRNAs as Biomarkers

Biomarkers have been developed as indicators for disease, monitoring clinical drug therapies or in toxicology. They are cellular or biochemical processes or responses that can be objectively measured (Strimbu & Tavel, 2010). Recently, microRNAs have been gaining popularity as candidate biomarkers within oncology, infectious diseases, autoimmune disease and many more (Filipów & Łaczmański, 2019; Tribolet et al., 2020; L. Zhang et al., 2020). A combination of biomarker screening during pregnancy also aims to detect perinatal complications. Adding novel biomarkers such as miRs, can improve screening methods and increase the range of complications that can be detected. miRs for detecting preeclampsia or fetal growth restriction have already been published (Mavreli et al., 2020; Tagliaferri et al., 2021; Yoffe et al., 2018). miRs have also been studied within different tissues to detect cellular toxicity (Schraml et al., 2017). For instance, miRs have been proposed as biomarkers for drug induced hepatotoxicity. In rats given toxic doses of acetaminophen two miRs were down-regulated and involved in regulating gene pathways for mitochondrial function and oxidative stress (Fukushima et al., 2007). For example, miR-222 has been identified in regulating toxicity related functions by indirectly suppressing superoxide dismutase-2 (SOD2) (Liu et al., 2009). While other miRs like miR-17, directly suppress antioxidant enzymes glutathione peroxidase-2 (GPX2), thioredoxin reductase-2 (TRXR2) and SOD2 (Xu et al., 2010). These examples, support the use of miRs as biomarkers for drug-induced toxicity or for monitoring drug safety. miRs can also

be used as biomarkers for development. One of the first studies for miRs in NC development was identified in *Xenopus laevis* where knockdown of miR-200b, miR-96 and miR-196a displayed craniofacial defects (Gessert et al., 2010). Later, (Du et al., 2013) showed in hESCs that the miRs observed in *Xenopus,* miR-200 and miR-96, are involved with suppressing neural differentiation by targeting *ZEB* and *PAX6*, respectively. Another group has differentiated hESCs into NCCs and came up with a mechanistic study showing differential expression of miR-29b inhibits NCC lineage specification by inhibiting DNA methyltransferase 3 alpha (*DNMT3A*) (J. Xi et al., 2017). Since then, many miRs have been identified or predicted to target genes involved with NCC specification, migration and differentiation (Sera & Zur Nieden, 2017). In addition, miRs also regulate differentiation of hESCs into mesoderm. Such miRs like miR-373, when overexpressed, led to the commitment of hESCs towards the mesodermal lineage. The target for miR-373 is *LEFTY,* which is involved with the TGFβ pathway, and its repression promoted differentiation into mesoderm (Rosa et al., 2014).

Bone Development

During embryonic development bones are formed from paraxial mesoderm, lateral plate mesoderm and NCCs (Nakashima & de Crombrugghe, 2003). In multiple vertebrate species (frog and chick embryos), the ectodermal germ layer expresses a combination of morphogenic signals at the time of gastrulation: *BMP*, *FGF*, *WNT* and *NOTCH*, which pattern the ectoderm into the neural plate (Merrill et al., 2006). At the neural plate border in response to these early signals, a set of transcription factors is activated (*ZIC1,TFAP2, MSX1, DLX5/6, PAX3/7,* and *GBX2*). The neural plate border forms NCCs, a transient stem

cell population that eventually forms various tissues. The cranial NCCs migrate to the pharyngeal arches where they from craniofacial cartilage, facial bones, bone of the middle ear, connective tissues of the face and odontoblasts of the teeth, that form and maintain dentin. The trunk NCCs migrate towards the mid ventral surface of the embryo to develop into melanocytes (Kunisada et al., 1998). Vagal and sacral NCCs migrate towards the neck region and form the enteric nervous system. Cardiac NCCs migrate from the cranial portion of the neural tube and go on to develop into neurons, cartilage, connective tissues of the arteries in the heart and cardiomyocytes (George et al., 2020; Le Douarin & Teillet, 1973; Le Lièvre & Le Douarin, 1975). The NCCs are then specified by expression of another set of genes (*SNAI1/2, TWIST1, FOXD3, SOX9, SOX10, ETS1*) (Simões-Costa & Bronner, 2015). These genes will downregulate cadherins and allow the NCCs to delaminate from the neural tube and migrate in a process called epithelial-to-mesenchymal transition (EMT) (Piacentino et al., 2020). The NCCs migrate towards the pharyngeal arches of the embryo, which leads to the formation of the craniofacial skeleton (McKinney et al., 2020).

In contrast, the axial skeleton (ribs, sternum, and vertebral column) is formed from paraxial mesoderm, whereas the appendicular skeleton (limbs and pelvis) is formed from lateral plate mesoderm. Both paraxial and lateral mesoderm lie adjacent to the neural tube, and a BMP gradient specifies the mesoderm subtypes (Pourquié et al., 1996; Tonegawa & Takahashi, 1998). For mesoderm to form, expression of *TBXT* (T-Box Transcription Factor T) early in the primitive streak and *TBX6* (T-Box Transcription Factor 6) is required. Loss of *TBXT* failed to form mesoderm within mouse embryos and loss of *TBX6* converted presomitic mesoderm into neural tissues (Gruneberg, 1958; Takemoto et al., 2011). For the

paraxial mesoderm to begin cell fate commitment (somite induction and subsequently sclerotome specification), expression of *MSGN1* (Mesogenin 1) is required; without it the body and tail in mice failed to form (Yoon & Wold, 2000). In somite induction *MSGN1* must be down-regulated and *MESP2* (Mesoderm Posterior BHLH Transcription Factor 2), *TCF15* (Paraxis), *PAX3*, *Foxc1/2* and *Meox1/2* are up-regulated (Chu et al., 2019; Kume et al., 2001; Mankoo et al., 2003; Matsuda et al., 2020; Nakajima et al., 2018; Saga et al., 1997). Next, sclerotome (a mesenchymal tissue) specification occurs with the expression of *Pax1*, *Pax9*, *NKX3-2* (Bapx1), and *Sox9* (Matsuda et al., 2020; Nakajima et al., 2018; H. Xi et al., 2017; Zhao et al., 2014). The sclerotome goes on to form the vertebrae, rib cage, and the lower part of the occipital bone.

Both the NCCs and specified mesoderm form migratory mesenchymal cell populations then are further committed to form bone though osteogenesis. Most NCCs differentiate through intramembranous ossification, and paraxial mesoderm primarily differentiates into bone though endochondral ossification, which forms a cartilage intermediate that is replaced by bone (Mackie et al., 2008). Commitment into the osteogenic lineage begins with the expression of the master regulatory transcription factors of the osteogenic lineage, Runt-related transcription factor 2 (*Runx2*/Cbfa1) and Osterix (*SP7*) (Komori et al., 1997; Nakashima et al., 2002; Otto et al., 1997). Through direct transcriptional activation these regulate expression of extracellular matrix proteins collagen type 1 (Col1) and osteocalcin that characterize osteoblast identity (Nakashima et al., 2002; Takarada et al., 2016; C. Zhang et al., 2008). Osteoblasts facilitate the initial mineral deposition by accumulating calcium and phosphate ions in the extracellular matrix.

Clusters of these ions come together to form the stable hydroxyapatite crystals, a hallmark characteristic of bone extracellular matrix mineralization.

Embryonic Stem Cell Differentiation

Embryonic stem cells (ESCs) are pluripotent stem cells derived from the inner cell mass of a blastocyst (4-day old embryo) (J. E. Lee & Lee, 2011). These cells can be directed to differentiate into any of the germ layers (ectoderm, mesoderm, and endoderm) and some even call the neural crest cells the fourth germ layer, because they have a developmental capacity mirroring that of a pluripotent cell. Because of their ability to form over 200 different cell types, ESCs are a useful *in vitro* model to study early development within humans. To study a specific form of development, in the current case osteogenic development, ESCs must be converted into the cell types involved with osteogenic development. This is done by manipulating the culture conditions to reduce cell pluripotency and increase signals that promote osteoblast development. This approach has been used to convert mouse ESCs into different cell types; neural cells, adipocytes, muscle cells and chondrocytes (Bain et al., 1995; Dani et al., 1997; Kramer et al., 2000; Rohwedel et al., 1994).

Some of the first studies differentiating cells into osteoblasts were conducted in murine embryonic mesenchymal cells (Katagiri et al., 1990). By adding supplements to the media such as, ascorbic acid, β-glycerophosphate or dexamethasone enhanced differentiation into osteoblasts (Cheng et al., 1994; Chentoufi et al., 1993; Franceschi & Iyer, 1992; Poliard et al., 1995). Other groups have added vitamin D_3 in combination with the above supplements to promote osteogenic differentiation in various cell types

(Beresford et al., 1994; Leboy et al., 1991). Later on, it was shown that addition of retinoic acid could be added to promote osteogenic differentiation from embryonic stem cells (Buttery et al., 2001; Phillips et al., 2001). Specifically, one group found that retinoic acid was able to promote differentiation of ESCs though the neural crest route (Kawaguchi et al., 2005). Our group has contributed significantly to the refinement of osteogenic culture conditions from ESCs using vitamin D_3 as the main osteogenic inducer (zur Nieden et al., 2003). Many of the mentioned supplements were also later tested in human ESCs and found to also be optimal for differentiating human cells into osteoblasts (Bielby et al., 2004; Kuske et al., 2011). Following a vitamin D_3-based protocol developed by our lab (Sparks et al., 2018), we have observed that neural crest gene markers (*PAX7, TFAP2A, ZIC3 and MSX2*) are significantly higher than the mesodermal gene markers (*TBXT and TBX6*) (Sparks et al., 2018). This shows that our differentiation protocol favors the neural crest lineage although both lineages were present in differentiation.

Embryonic Stem Cell Test and Toxicity Screening

In vitro assays have been developed to predict developmental toxicity of chemical or drug exposure. One such example is the embryonic stem cell test (EST), which was first described by Spielmann and colleagues (Spielmann et al., 1998) and then fully validated with 20 compounds (Scholz et al., 1999). The test measures three endpoints and classifies a chemical as embryotoxic if (1) the concentration of the chemical inhibits 50% of the cells from differentiating (ID_{50}), (2) there is a 50% decrease in cell viability of ESCs (IC_{50}) and (3) there is a 50% decrease in viability of mature somatic cells (fibroblasts)(IC_{50}). Developed to test for cardiac embryotoxicity, since its initial inception, the EST has been

transferred to many additional tissue endpoints, among them skeletal development, by employing osteogenic differentiation protocols as outlined above (Walker et al., 2014; zur Nieden & Baumgartner, 2010; zur Nieden et al., 2004).

Initially, murine embryonic stem cells (mESCs) were used in the EST to test for the embryotoxicity of a chemical. However, using human ESCs would better predict effects on humans and remove any interspecies differences, as it has been shown that non-human primates responded differently to toxicants than mESCs (Walker et al., 2014). In prior work, our lab showed that the human osteogenic EST (hESTo) correctly classified 13-*cis*-retinoic acid, a human teratogen with lesser effects in the mouse, as a moderate embryotoxicant, thus underlining the superiority of a human-based cell assay. In addition, the calcification endpoint correctly classified a set of selected chemicals known to negatively affect neural crest and mesoderm osteogenesis.

The toxicants used in this prior study displayed developmental defects in the craniofacial skeleton and axial skeleton, attributed to neural crest and mesoderm development, respectively. The chemicals cyclopamine, methoxyacetic acid, ogremorphin and triadimenol were selected for their inhibition of neural crest differentiation (Brown et al., 1984; Dunn et al., 1995; Zimmer et al., 2012). The toxicants cyclophosphamide, methotrexate and valproic acid were used for their displayed inhibition to mesoderm differentiation (de Leeuw et al., 2020; Hyoun et al., 2012; Meisig et al., 2020; Sahakyan et al., 2017; Vaux et al., 2003; Zhu et al., 2011). Some of these chemicals have overlapping effects, perturbing both NC and mesoderm differentiation. For example, valproic acid interferes with NCC motility and mesodermal differentiation (Fuller et al., 2002; Murabe

et al., 2007). The concentrations of these chemicals used in this study were established with the human EST.

Bioinformatic Analysis of MicroRNAs

In the field of toxicology, many previous studies have applied qPCR or microarray techniques to identify novel regulatory miRNAs (Fukushima et al., 2007; Marsit et al., 2006; Pogribny et al., 2007; Sathyan et al., 2007). Next generation sequencing has been applied more recently due to improved availability of equipment, increasingly lower costs and its superior ability to detect sequences that are un-defined, such as in microarray techniques (Mestdagh et al., 2014). One of the most important steps to microRNA analysis is the isolation of small RNAs. This is commonly achieved with kits that purify total RNA and perform size selection to enrich for small RNAs (Wong et al., 2019). The next step is to sequence and analyze the reads. Many software tools exist to aid in microRNA analysis; however, they mainly rely on open-source tools packaged together. For example, miRDeep2 uses a choice of bowtie or BWA as the read aligner (Friedländer et al., 2012). The alignment step is another important step as it is a little different from traditional mRNA alignment. The choice of aligner and parameters can have an effect on accurately aligning reads and on the significance of the downstream differential miR expression (Ziemann et al., 2016). Since microRNAs can align to multiple distinct locations the alignment parameters must account for this. Depending on the aligner used a multimapping parameter is specified to account for this. For example, human miR-1302 can be mapped to 11 genomic locations (Yuan et al., 2010). After alignment, annotation and read counting is performed. For annotating microRNAs the database miRbase (Kozomara et al., 2019) is

commonly used, as it is constantly updated and curates microRNAs with 'high confidence' (Kozomara & Griffiths-Jones, 2014). Differential expression of the microRNA datasets is commonly conducted with R packages, such as edgeR and DESeq2 (Capece et al., 2015; L. Chang & Xia, 2023; Hackenberg et al., 2011; Rueda et al., 2015).

Once differentially expressed miRs have been identified their target mRNAs can be computationally predicted or obtained from annotated databases that have curated experimentally validated miRNA-target interactions from publications. Efforts to integrate microRNA-seq and RNA-seq data have been used to show a functional relationship and narrow down context specific targets. Different approaches have been taken to integrate the two datasets, most of them use correlation analysis to compare the miR and its differentially expressed target (Nersisyan et al., 2020; Patel et al., 2021; T.-T. Wang et al., 2019; Yao et al., 2019). With the aid of Shiny (W. Chang et al., 2022), an R package that can execute R code in a web application, visualization of microRNA and mRNA datasets can be run interactively. Users can interact with the dataset and choose to plot different treatment combinations, visualize different filtering cutoffs and perform calculations that would not be easily done by non-bioinformaticians. Within a Shiny app correlation analysis can be performed to integrate the datasets and perform functional analysis to find biological function of miR-mRNA pairs.

Goal of the Study

While the hESTo successfully identified chemicals with a propensity to inhibit osteogenic differentiation in general, as of yet, there is no assay that can detect differences in the skeletal lineages that are targeted by such chemicals. The goal of this study, therefore,

is to develop a set of miR biomarkers that correlate with neural crest and mesoderm toxicity, respectively. To achieve this goal, human ESCs (hESCs) will be taken through osteogenic differentiation and exposed to each of these individual toxicants. Bioinformatic analysis of miR expression profiles will then allow an assessment of differentially expressed miRs involved with either facial or limb skeletal development, or potentially both.

The underlying hypothesis is that the commitment of the cell to either the neural crest or mesoderm lineage may be affected by different miRs. To perturb a specific lineage and assess the miRs within each lineage, toxicants that have demonstrated defects in neural crest and mesoderm differentiation were selected. The specific focus of this work is to develop an app that can facilitate interpretation and visualization of microRNA-seq and RNA-seq datasets. There are many free-standing web apps that can take sequencing data and perform basic analysis and visualizations. However, there is a need to develop an app that can accommodate the analysis of different treatment combinations and integrate the analysis between two sequencing datasets. This can be accomplished by using R Shiny, which can build a web application letting users interact with the data, to select significant results and graph them quickly, without knowing the technical aspects of coding.

Materials and Methods

Cell Culture and Differentiation

Human embryonic stem cells (H9) acquired from WiCell (WiCell Research Institute), were cultured on Matrigel (BD Biosciences) treated dishes and maintained as

feeder-free cultures in mTeSR® media (Stem Cell Technologies) in 5% CO_2 and at 37°C. Cultures were routinely checked for mycoplasma contamination (ATCC, Cat no. 30-1012K). Pluripotent colonies were passaged every 4-5 days upon reaching 70% confluency by dissociating cells with ACCUTASE™ (Stem Cell Technologies) and a cell scraper (Madrid et al., 2018). H9 confluent colonies designated as day 0 were switched to control differentiation medium composed of Dulbecco's Modified Eagle's Medium (DMEM, Gibco) 15% FBS (Atlanta), 1% non-essential amino acids (NEAA; Gibco), 1:200 penicillin/streptomycin (Gibco), and 0.1 mM β-mercaptoethanol (Sigma). On day 5, the control differentiation medium was supplemented with 10 mM β-glycerophosphate (Sigma), 25 µg/ml ascorbic acid (Sigma), and 50 nM 1,25$(OH)_2$ Vitamin D_3 (Calbiochem) (Sparks et al., 2018).

Test Chemicals and Exposure

The test chemicals in table 1 were selected for their known developmental inhibitory effects on neural crest and mesoderm development. 5-fluorouracil (5-FU) is used as positive control for general embryo- and developmental toxicity and for its ability to inhibit cell proliferation and differentiation (Focaccetti et al., 2015; Ghafouri-Fard et al., 2021; Yamada et al., 2018). The concentrations were previously determined by their effects on differentiation (Ca^{2+}) using concentration-response curves, then the half-maximal inhibitory concentrations ($ID_{50}Ca^{2+}$) of for each compound were linearly interpolated from the curve using GraphPad Prism. Test chemicals were acquired from the manufacturers as specified in table 1 and either dissolved in DMSO or PBS, based on their solubility. Test chemicals were added on day 0 of differentiation and remained until the endpoint of the

experiment (day 7). All compounds were replenished with each media change performed every two days. A solvent control containing the highest concentration of solvent was included to control for non-chemical specific effects .

Chemical	µM	µg/mL
Cyclopamine (CYCLO) Millipore Sigma CAS# 4449-51-8	100	41.16
Methoxyacetic acid (MAA) Millipore Sigma CAS# 625-45-6	100	9
Ogremorphin (OGM) kindly provided by Dr. Charles Hong (Vanderbilt University)	0.1	0.0309
Triademenol (MENOL) Millipore Sigma CAS# 55219-65-3	100	25.58
Cyclophosphamide (CPA) ThermoFisher CAS# 6055-19-2	35.8	10
Methotrexate (MTX) Alfa Aesar CAS# 59-05-2	0.022	0.01
Valproic acid (VPA) R&D Systems CAS# 1069-66-5	58.9	10
5-Flurouracil (5-FU) Millipore Sigma CAS# 51-21-8	0.0192	0.0025

Table 1: Toxicants used in treatments

RNA Extraction and Library Preparation

Cells were taken through osteogenic differentiation until day 7 of the differentiation protocol, a time point at which early neural crest markers (*PAX7, TWIST1* & *SOX10*) are up-regulated (Sparks et al., 2018). Then cell cultures were lysed in 500 µL of QIAzol lysis reagent (Qiagen, Cat. No.: 79306) and disrupted by cell scraping and pipetting. miRNA and total RNA from the same sample were purified and concentrated according to the miRNeasy and RNeasy MinElute Cleanup Kits (Qiagen). Samples were assessed for RNA quality with the Bioanalyzer 2100 (Agilent) at the Genomics Core Facilty at UC Riverside and taken through library prep if RIN values were greater than 9. Following the protocol for the NEBNext® Multiplex Small RNA Library Prep Set for Illumina (NEB, Cat No.: E7330), 100 ng of each miRNA and RNA sample, quantified by the NanoDrop spectrophotometer (Thermo Scientific), was used as input for library preparation. Initial

miRNA library size selection was done on a 6% PAGE gel, visualized with Sybr Gold, at ~140 bp. This corresponds to the adapter-ligated constructs (21 nt RNA fragments and adapter). For mRNA sequencing, first the ribosomal RNA was depleted using the NEBNext® Poly(A) mRNA Magnetic Isolation Module (NEB, Cat No.: E7490). Then the libraries were constructed using NEBNext® Ultra™ II Directional RNA Library Prep Kit for Illumina (NEB, Cat No.: E7760). To summarize these steps, first the RNA was fragmented, then first strand cDNA was generated followed by second strand cDNA. The ends of the cDNA were repaired (dA-tailing) then the NEBNext Adaptor was ligated to the cDNA with NEBNext Ultra II Ligation Master Mix and the reaction was purified with NEBNext Sample Purification Beads (supplied in kit). The libraries were then amplified by PCR (12 cycles) with the index/i7 primer (5'-CAAGCAGAAGACGGCATACGA-3') and Universal PCR Primer/i5 primer (5'-ATGATACGGCGACCACCGAGATCTACACTCTTTCCCTACACGACGCTCTTCCGATC-3'). The reaction was then purified with SPRIselect Beads (in kit NEB, Cat No.: E7760) and assessed for quality on the Agilent Bioanalyzer DNA chip. Libraries were found of appropriate quality when the Bioanalyzer electropherogram showed a distribution peak size at approximately 300bp in the absence of primer or adaptor-primer peaks (~80 bp and 128 bp, respectively).

MiRNA Sequencing Analysis

Resulting libraries were sequenced on the Illumina NextSeq 550 High Output 1 x 75 (Single-end) for an average of 22 million reads at the UCR Genomics Core Facility. After sequencing, fastq files were assessed for read quality and length using Fastqc

(0.11.7). Reads with base quality less than 20 and sequences with length less than 18 bp were trimmed and discarded using Trimmomatic (0.36). Reads were then aligned to the indexed human genome GRCh38, using the Bowtie (1.2.2) short read aligner with the parameters: "bowtie -a --best --strata -m 10 -l 10 -S HS_index output.sam". Reads were quantified using featureCounts in the Subread package using the miRbase (Release 22.1) human feature format file (hsa.gff3) with the following parameters: "featureCounts -t miRNA -g Name -O -s 1 -M -a hsa.gff3 -o <outfile> <samfiles>". The quantified reads were normalized using the DESeq2 (1.36.0) normalization (median of ratios). Differential analysis was performed with DESeq2 (1.36.0). Both normalized counts and differential analysis results were then imported into the R Shiny (1.7.2) app.

MRNA Sequencing Analysis

Libraries were sequenced on the Illumina NextSeq 550 High Output 1 x 75 (Single-end) for an average of 23 million reads at the UCR Genomics Core Facility. Read quality was assessed with Fastqc (0.11.7). Alignment was performed with Hisat2 (2.1.0) to the indexed human genome GRCh38, and samtools (1.10) was used to sort and convert to bam files. Counts were generated with featureCounts from the subread (2.0.1) package. Count normalization and differential analysis was performed with DESeq2 (1.36.0). The normalized counts and differential analysis results were used in the R Shiny (1.7.2) app.

Shiny App

A shiny app is a web interface that executes R code in the backend. The app developed in our lab uses the normalized counts dataframe and a list of dataframes containing differential expression for each toxicant, as inputs for the visualization,

functional annotation, and correlation analysis. The user interface (UI) components of the app, sidebar, header, tabs and body layout are within the app.R script. The second part of the script contains the server functions containing reactive functions for processing the counts and differential expression, such as filtering by toxicant, foldchange cutoffs and p-adjusted value cutoffs. Plots and tables are rendered in the server function and output in the UI. The normalized count data was used in the boxplots, heatmaps and Pearson correlation calculations. The differential expression data is used to generate volcano plots, radar plots and gene ontology (GO) analysis. The app is hosted on shinyapps.io (https://willdesi.shinyapps.io/mirTox-App/) with up to 8 GB of memory and was created with the below R (version 4.2.1) packages (Table 2). All code is available on a Github repository (https://github.com/dwill023/mirTox-App).

package	loadedversion	date	source
AnnotationDbi	1.58.0	2022-04-26	Bioconductor
Biobase	2.56.0	2022-04-26	Bioconductor
BiocGenerics	0.42.0	2022-04-26	Bioconductor
bs4Dash	2.1.0	2022-05-05	CRAN (R 4.2.1)
clusterProfiler	4.4.4	2022-06-21	Bioconductor
DOSE	3.22.1	2022-08-30	Bioconductor
dplyr	1.0.10	2022-09-01	CRAN (R 4.2.1)
ds4psy	0.8.0	2022-04-07	CRAN (R 4.2.1)
DT	0.24	2022-08-09	CRAN (R 4.2.1)
EnhancedVolcano	1.14.0	2022-04-26	Bioconductor
fmsb	0.7.3	2022-03-01	CRAN (R 4.2.1)
fresh	0.2.0	2020-05-29	CRAN (R 4.2.1)
ggplot2	3.3.6	2022-05-03	CRAN (R 4.2.1)
ggpubr	0.4.0	2020-06-27	CRAN (R 4.2.1)
ggrepel	0.9.1	2021-01-15	CRAN (R 4.2.1)
gt	0.7.0	2022-08-25	CRAN (R 4.2.1)
htmlwidgets	1.5.4	2021-09-08	CRAN (R 4.2.1)
IRanges	2.30.1	2022-08-25	Bioconductor
matrixStats	0.62.0	2022-04-19	CRAN (R 4.2.1)
miRNetR	0.0.0.9000	2022-09-01	Github (xia-lab/miRNetR@cab41bf57bfe0dff5ab7c27e77b9bd3ff0dd279e)
org.Hs.eg.db	3.15.0	2022-09-02	Bioconductor
paletteer	1.4.1	2022-08-15	CRAN (R 4.2.1)
pheatmap	1.0.12	2019-01-04	CRAN (R 4.2.1)
plotly	4.10.0	2021-10-09	CRAN (R 4.2.1)
ReactomePA	1.40.0	2022-04-26	Bioconductor
S4Vectors	0.34.0	2022-04-26	Bioconductor
shiny	1.7.2	2022-07-19	CRAN (R 4.2.1)
shinycssloaders	1.0.0	2020-07-28	CRAN (R 4.2.1)
shinycustomloader	0.9.0	2018-03-27	CRAN (R 4.2.1)
shinyjs	2.1.0	2021-12-23	CRAN (R 4.2.1)
shinyWidgets	0.7.3	2022-08-31	CRAN (R 4.2.1)
tippy	0.1.0	2021-01-11	CRAN (R 4.2.1)
unikn	0.5.0	2022-08-15	CRAN (R 4.2.1)
upsetjs	1.11.1	2022-07-13	CRAN (R 4.2.1)
viridis	0.6.2	2021-10-13	CRAN (R 4.2.1)
viridisLite	0.4.1	2022-08-22	CRAN (R 4.2.1)

Table 2: R packages and versions used in the Shiny app.

Within the app, microRNA validated targets were obtained from three databases miRTarBase v8.0, TarBase v8.0 and miRecords with the miRNetR package . The validated targets were used in over representation analysis (ORA) (Boyle et al., 2004) using clusterProfiler within GO terms available in five databases; Kyoto Encyclopedia of Genes and Genomes (KEGG), Reactome, Disease Ontology (DO) (Schriml et al., 2012), GO:

Biological Processes, and WikiPathways. microRNA targets were correlated with the differentially expressed mRNAs. All results were generated using a log2-fold-change-cutoff of 0.5 and a false discovery rate (p-adjusted value) at 0.05. The correlations were calculated using the DESeq2 normalized counts to allow comparisons between samples. The normalized counts were scaled with a $\log_2$-transformation ($\log_2$(count+1)), then a Pearson correlation was calculated for the miR-mRNA pair. When multiple toxicants are selected, the correlation for the miR-mRNA pair is calculated across all toxicants.

Results and Discussion

To identify neural crest and mesoderm-toxicity-associated miRNAs and potential mRNA targets they regulate, an R Shiny app was developed to facilitate user friendly analysis. App design, surface and workflow shall be presented followed by a selection of major results presenting differentially regulated miRs, mRNAs and potential miR-mRNA networks.

Application Design and Workflow

The miRTox app (https://willdesi.shinyapps.io/mirTox-App/) was developed to facilitate the analysis of both microRNA and mRNA sequencing datasets and easily integrate them to identify microRNA-mRNA correlated pairs. The UI of the app is arranged into five sections in the sidebar (Appendix Fig. S1). The first section introduces the objective, experimental approach, and treatment conditions (Appendix Fig. S1). The microRNA expression section takes the normalized count data and allows users to select a miR of interest and view the expression in the form of boxplots and in an adjacent table (Appendix Fig. S2A). The differential expression data is displayed by selecting the toxicant and viewed in a volcano plot. The initial selected miR for the boxplots is also highlighted in the volcano plot. Thresholds for fold-change and p-values for the differential expression can be adjusted by clicking the cog icon in the volcano plot box (Fig. S2B). All points meeting the selected thresholds in the volcano plot are also displayed in the adjacent table. An upset plot is used to view overlapping miRs within multiple toxicant treatments, users can select different treatments and the direction of the differential expression (up or down-regulated) (Appendix Fig. S2C). A list of the overlapping miRs can be displayed by

clicking the overlap of interest. These miRs are also shown in an adjacent table with their log2FoldChange and p-values. Thresholds for these can also be adjusted in the upset plot within the cog (settings) icon of the box (Appendix Fig. S2C). Heatmaps are also available to show the overall expression of the miRs within user selected treatments. They are generated using the normalized counts and in the tabs there's a choice to generate heatmaps for the median expression or for user selected miRs (Appendix Fig. S3A). Radar plots are available to help compare miRs within selected toxicants or comparing a miR across multiple toxicants (Appendix Fig. S3B). These are generated using the differential expression. The last box in the microRNA section allows the user to generate the microRNA targets by choosing the toxicant then parameters for the miR used in generating the mRNA targets (Appendix Fig. S4A). There is also an option to input a custom list of miRs such as those generated from the overlaps in the upset plot. Once the mRNA targets are generated, a new tab will appear to allow users to choose the ontology database to get functional annotations for the targets (Appendix Fig. S4B). These functional annotations can be plotted in a dot plot or bar chart in the adjacent tabs (Appendix Fig. S4C). These same analysis and visualizations are available for the mRNA-seq data in the mRNA expression section.

The last section, Correlation Analysis, was specifically created to determine the strength of the relationship between differentially expressed miRs and differentially expressed mRNAs that they target. The user is able to choose the toxicant, direction of fold change, and significance cutoffs to obtain microRNA targets that are differentially expressed in the mRNA-seq data. These mRNAs from the selected toxicants are plotted in

an upset plot and upon clicking a column in the upset plot the adjacent table displays the intersection, the differentially expressed mRNA and the corresponding miR (Appendix Fig. S5A). The mRNAs in the table are used in the next box to obtain functional annotation from a choice of five ontology databases (Appendix Fig. S5B). In the below box a table of correlations can be generated by choosing from the gene ontology that was generated in the above box or a list of the mRNA targets can be entered by choosing the custom option (Appendix Fig. S6A). This option allows users to copy the mRNA targets from the upset plot if no gene ontologies were generated or if only a small number of mRNAs are available. Pearson correlations for each miR and mRNA target are calculated across all toxicants if more than one is selected at the top of the page. The correlation table can be sorted by the correlation column (second last column). Since microRNAs negatively regulate its target mRNA, negative correlations can be used to identify pairs of miR-mRNA as potential biomarkers. For example, when a miR is observed to be up-regulated and its validated mRNA target down-regulated (or vice versa) a negative correlation below -0.5 with a p-value below 0.05 is used to identify a miR-mRNA pair. This approach has been taken by many others to integrate miRNA and mRNA data to identify and characterize their interactions (Cattane et al., 2022; Kumar et al., 2018; Patel et al., 2021; L. Wang et al., 2018; Yao et al., 2019). To plot the correlation for a selected miR-mRNA pair, clicking a row in the correlation table will generate the correlation plot in the box below the table (Appendix Fig. S6B).

MicroRNA Tab

Analyzing the miRNAs separately will help narrow down potential miRs that can act as biomarkers within differentiation and developmental pathways of interest. First, the miRs that were up or down-regulated in all toxicants were filtered. Next, the intersecting miRs were obtained. This approach was also performed separately on the neural crest toxicants (NC toxicants) and the mesoderm toxicants to identify miRs specific to NC and mesoderm cell differentiation. Validated miRNA-target interactions (MTI) were then obtained from the app in the miRNA expression tab fed from the three databases miRTarBase v8.0, TarBase v8.0 and miRecords. MTIs of intersecting up-regulated miRs in all treatments contained 21 miRs (Fig. 1A). These respective mRNA targets were then used in gene ontology (GO) analysis within the WikiPathways database. We observed pathways related to Wnt signaling, mesodermal commitment pathway and bone development (Fig. 1B). A table of the validated targets and the miRs that target them are given in appendix table 1.

In contrast, in the upset plot (Figure 1A) within all toxicants without 5-FU there are only 10 miRs. These miRs represent the effects of all toxicants without the pan-cellular toxicity displayed by 5-FU. Therefore, these 10 miRs should be characteristic for more specific lineage defects. Obtaining the mRNA targets and GO analysis revealed that the targets are involved with neural crest cell migration, Wnt signaling and osteoblast differentiation (Fig. 1C). Three miRs target the validated mRNAs involved with neural crest cell migration: miR-148a, miR-30a and miR-7. A full list of the gene ontologies are listed in appendix table 2.

The down-regulated miRs intersecting all toxicants contained a total of 44 miRs (Fig. 2A). Their MTIs are involved in both neural crest cell migration and mesodermal commitment (Fig. 2B). The down-regulated miRs that intersect the toxicants without 5-FU, contained 5 miRs and their associated MTIs are involved with mesodermal commitment (Fig. 2C). The miRs that target these mRNAs are miR-211, miR-195, miR-483 and miR-93. Some of the genes important to mesodermal commitment are *SNAI1, SMAD3, BMPR2, FZD8 and AXIN2.*

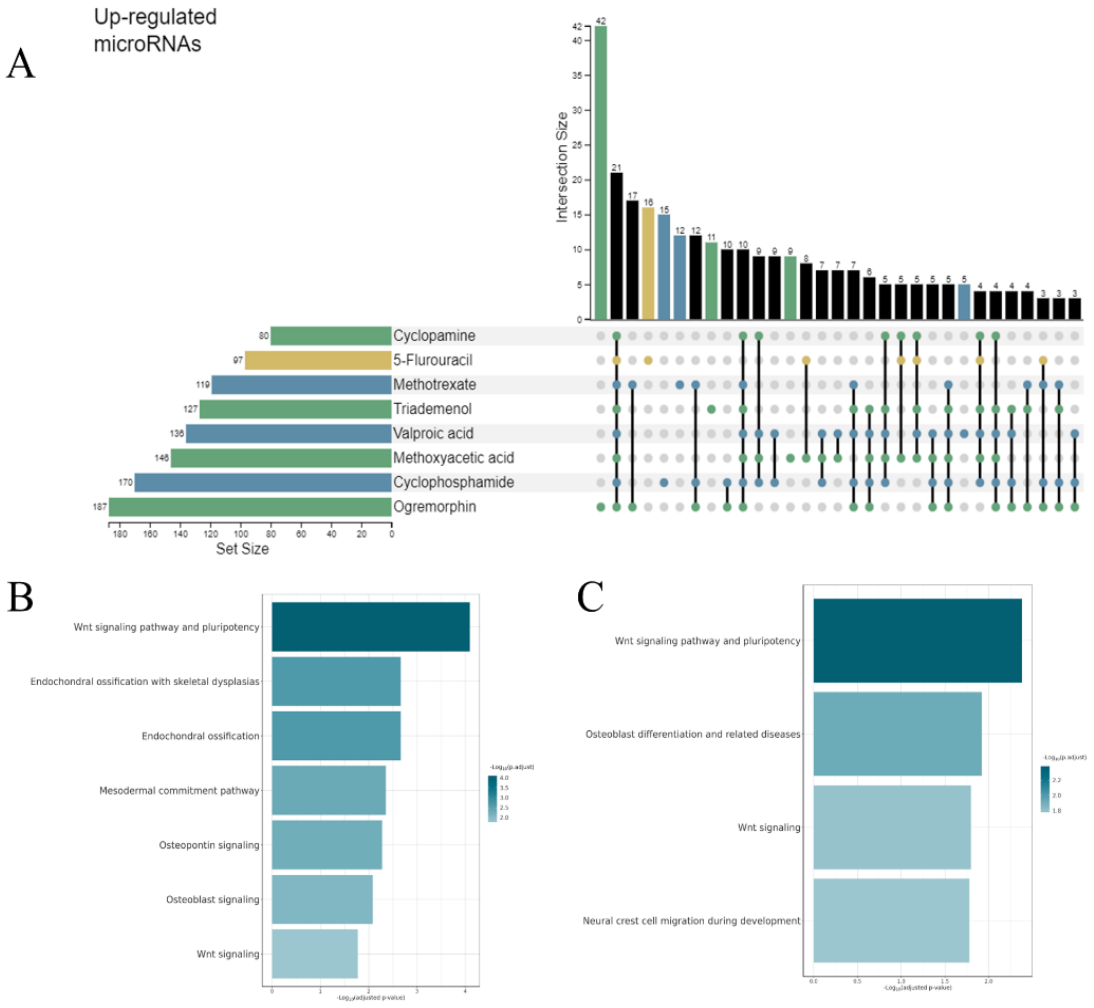

Figure 1: Up-regulated miRs in all toxicants
(A) Upset plot for the up-regulated miRs. Blue is for the mesoderm toxicants and green is for neural crest toxicants. When multiple toxicants overlap the color is black in the upset bars. (B) GOs generated from the 21 miRs overlapping all toxicants. (C) GOs for the 10 miRs overlapping all toxicants without 5-FU.

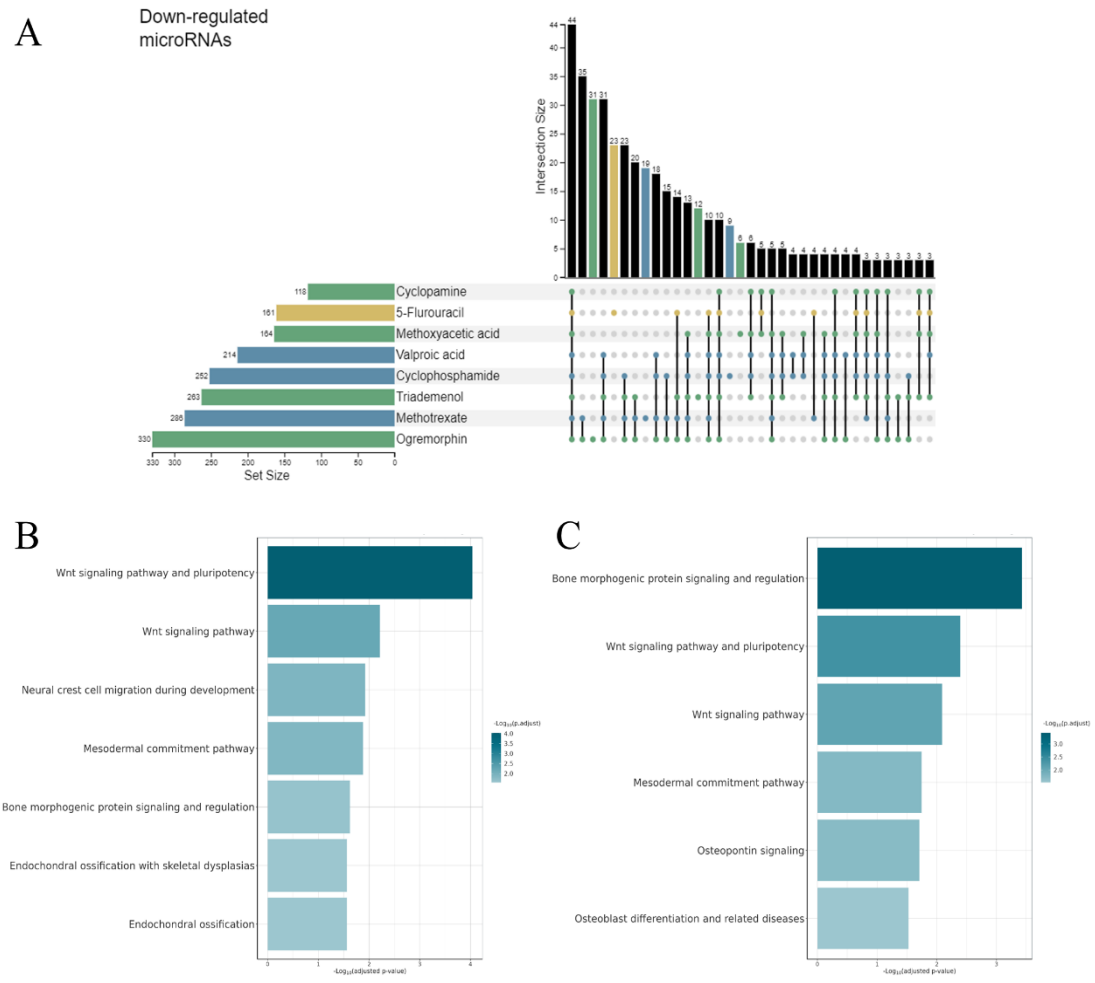

Figure 2 : Down-regulated miRs in all toxicants.
(A) Upset plot for the down-regulated miRs. Blue is for the mesoderm toxicants and green is for neural crest toxicants. When multiple toxicants overlap the color is black in the upset bars. (B) GOs for 44 miRs overlapping all toxicants. (C) GOs for 5 miRs overlapping all toxicants without 5-FU.

To narrow down effects specific to neural crest differentiation, the NC toxicants (cyclopamine, methoxyacetic acid, ogremorphin and triadimenol) were then overlapped to isolate miRs expressed within these toxicants only. With all NC toxicants, there were 26 up-regulated miRs (Fig. 3A) and their miRNA-target interactions are involved in select GO pathways related to osteogenic differentiation, mesodermal commitment, Wnt signaling and bone development (Fig. 3B). However, when it is exclusively NC toxicants there are

14 overlapping miRs (Fig. 3A) and the target mRNAs display a neural crest cell migration GO, not observed when 5-FU was included (Fig. 3C). These results supported what has been published previously, namely that these toxicants display developmental toxicities related to neural crest differentiation (Brown et al., 1984; Dunn et al., 1995; Zimmer et al., 2012). Out of the 14 miRs, half of them (miR-30a, miR-148a, miR-7, miR-146a, miR-146b, miR-4741 and miR-6868) target the genes involved in the GO neural crest migration. Down-regulated miRs among the NC toxicants were also overlapped (Fig. 3D), identifying 56 miRs overlapping in all toxicants and the miRNA-target interactions are involved in the select GOs bone, mesoderm, and neural crest development (Fig. 3E). There were 11 miRs specific to NC toxicants and those have MTIs with GOs in Wnt signaling, mesoderm and bone development (Fig. 3F).

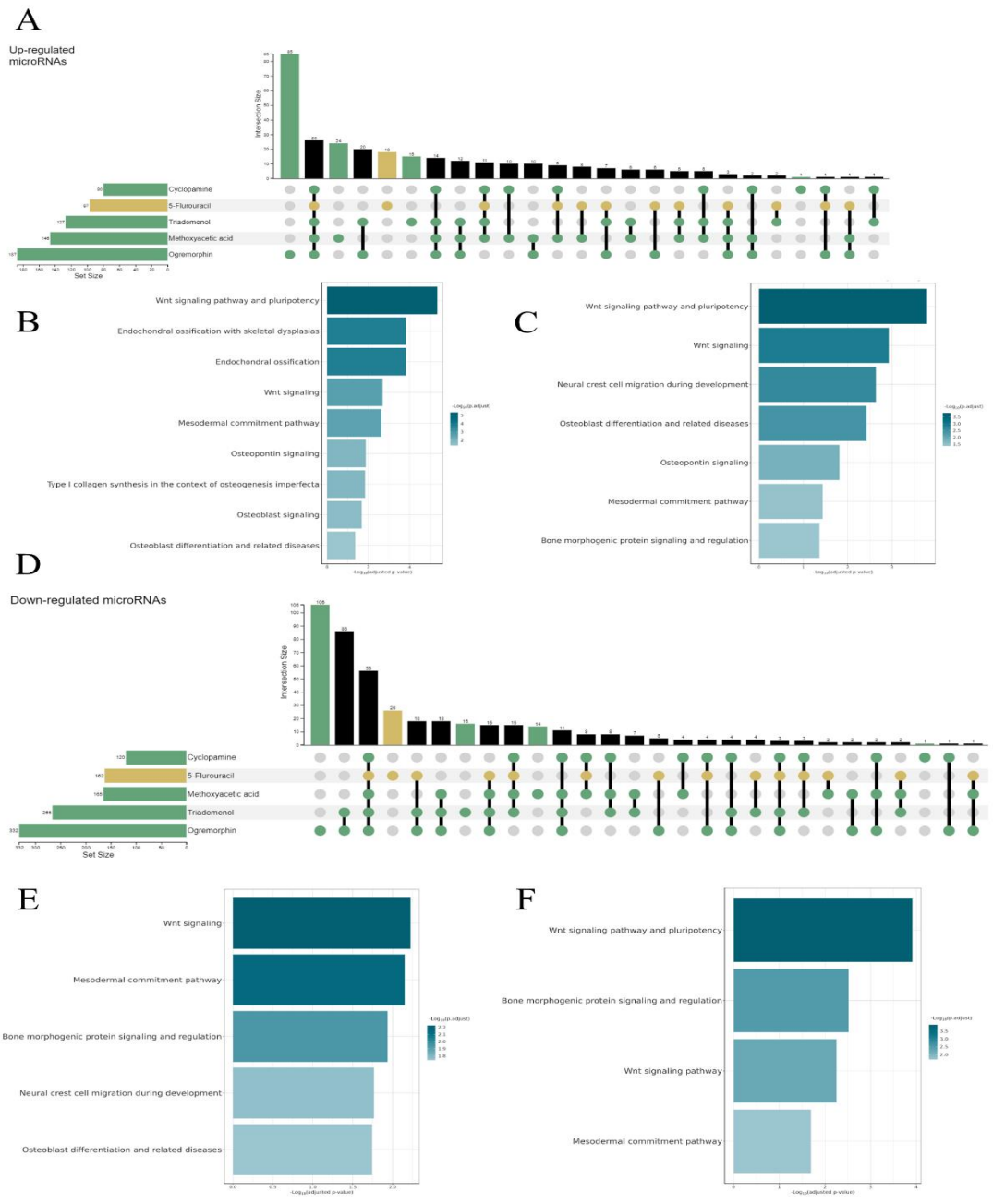

Figure 3 : microRNAs within neural crest toxicants.
(A) Upset plot for up-regulated miRs overlapping NC toxicants. (B) Select GOs for 26 miRs overlapping all toxicants. (C) Select GOs for 14 miRs overlapping NC specific toxicants only. (D) Upset plot for down-regulated miRs. (E) Select GOs for 56 down-regulated miRs overlapping all toxicants. (F) Select GOs for 11 down-regulated miRs overlapping NC specific toxicants only.

To narrow down miRs specific for mesoderm development, the toxicants cyclophosphamide, methotrexate and valproic acid were overlapped. There were 22 up-regulated miRs among all toxicants (Fig. 4A) and their miRNA-target interactions were involved with the GOs listed in Figure 4B, among them was mesodermal commitment pathway. In exclusively mesoderm toxicants, they have 27 overlapping miRs with MTIs involved with both mesodermal commitment, neural crest migration and bone development (Fig. 4C). The miRs within the mesoderm exclusive toxicants contain MTIs for neural crest cell migration, which indicate that there was some overlap between the miRs or mRNAs these toxicants affect and the NC toxicants.

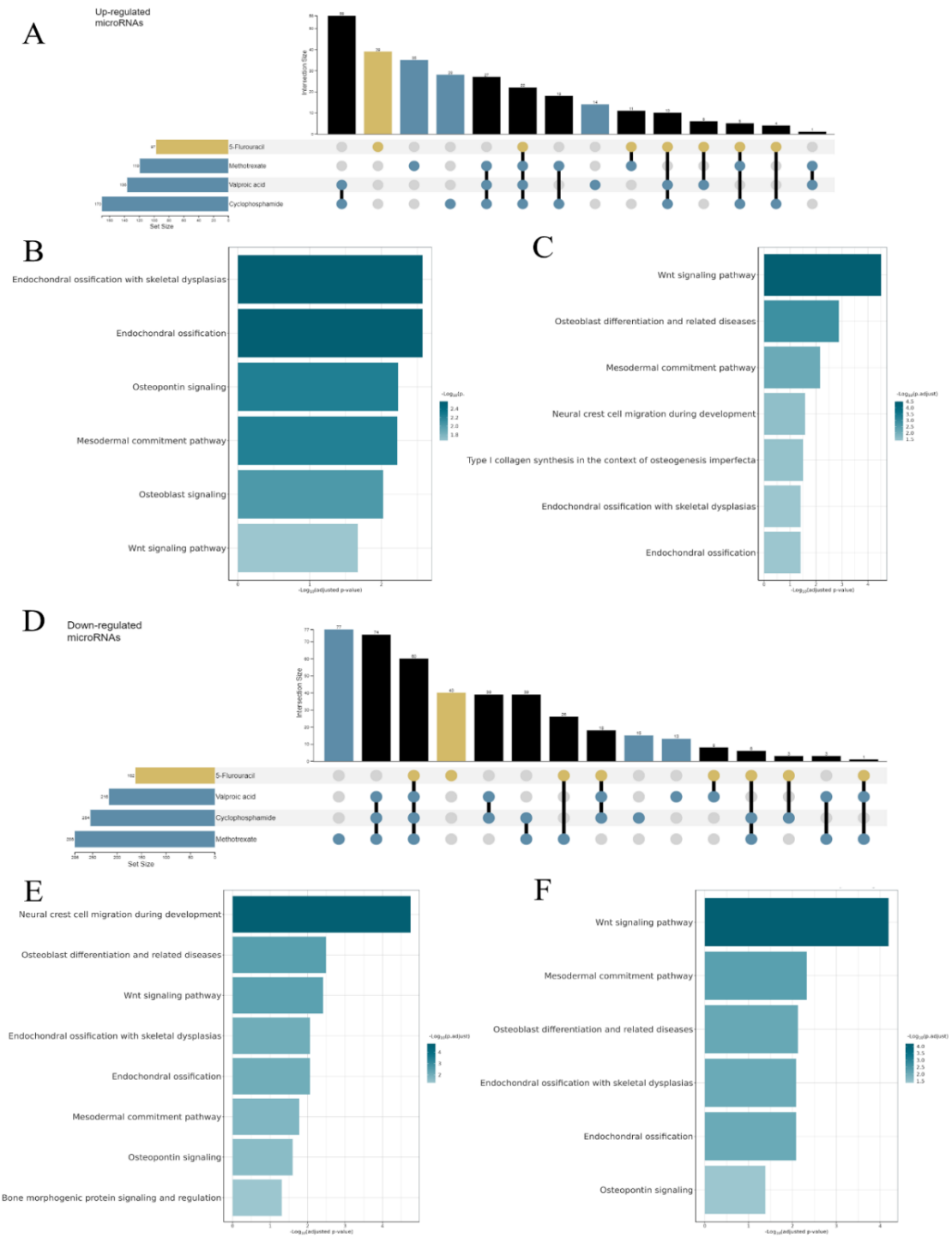

Figure 4 : microRNAs within mesoderm toxicants

(A) Upset plot for up-regulated miRs overlapping toxicants. (B) Select GOs for 22 miRs overlapping all toxicants. (C) Select GOs for 27 miRs overlapping toxicants without 5-FU. (D) Upset plot for down-regulated miRs. (E) Select GOs for 60 down-regulated miRs overlapping all toxicants. (F) Select GOs for 74 down-regulated miRs overlapping toxicants without 5-FU.

In addition, down-regulated miRs were overlapped and 60 of them intersected in all toxicants (Fig. 4D). The associated MTIs were enriched in the gene ontologies neural crest migration, mesodermal commitment pathway, bone development and Wnt signaling. (Fig 4E). In the exclusively mesoderm toxicants, there were 74 miRs intersecting. The MTIs for these miRs were involved with similar GO terms to the ones that included the positive control (5-FU), but the mesodermal commitment GO exhibited a greater significance (p-adjusted = 0.005). The mesodermal commitment GO was also significant within the up-regulated miR targets supporting the notion that these toxicants might have a role in mesoderm development and differentiation.

Since we have observed similar GO pathways in the up-regulated miRs of NC toxicants and the mesoderm toxicants, we chose to compare the GOs of neural crest cell migration during development between these groups of toxicants to see if there were any group specific MTIs. In this comparison, we identified three mRNA targets specific to the NC toxicants and three for the mesoderm toxicants (Fig. 5A). The miRs that target these mRNAs are listed in Figure 5C. There are 11 targets (*BDNF, JUN, PIK3CD, TRIO, STAT3, FOS, PAK1, PIK3CB, PIK3CG, PIK3R3,* and *AKT3*) that intersect all. We observed a shared GO, mesodermal commitment pathway, within the down-regulated miRs. By comparing the MTIs between the NC toxicants and mesoderm toxicants we observed 66 MTIs unique to mesoderm toxicants (Fig. 5B). A list of the gene targets is given in Figure 5D. In sum, the miRs identified to be specific for the two toxicant groups may be potential biomarkers for neural crest and mesoderm differentiation, respectively. The next step

would be to determine if the mRNAs are significantly regulated within the treatments or by validating the specific miR-mRNA interaction through microRNA knockdown .

A

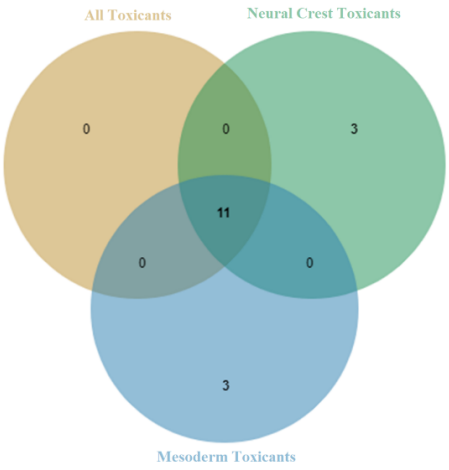

B

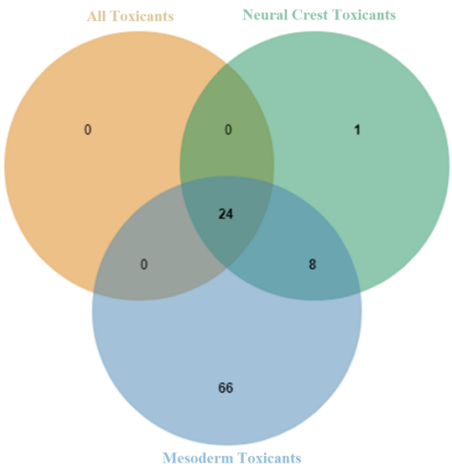

C

Neural crest cell migration during development			
Treatment	Target	Up regulated microRNA	PMID
Neural Crest Toxicants	RHOA	hsa-mir-146a-5p, hsa-mir-146b-5p, hsa-mir-4741	27175941, 23622248, 23592263|26701625
	RAC1	hsa-mir-146a-5p	25214035
	EPHB1	hsa-mir-6868-3p	23824327
Mesoderm Toxicants	AKT1	hsa-mir-126-3p, hsa-mir-184, hsa-mir-206, hsa-mir-27a-5p, hsa-mir-378c, hsa-mir-378d, hsa-mir-378f	26659078, 27666871, 28386239, 23963114, 21572407, 21572407, 21572407
	AKT2	hsa-mir-126-3p, hsa-mir-184	20371350, 20409325|20371350|27418134
	TWIST1	hsa-mir-206, hsa-mir-151a-3p	26272918, 27930738

D

Mesodermal commitment pathway	
Treatment	Down regulated miR Targets
Neural Crest Toxicants	NCAPG2
Mesoderm Toxicants	ACACA, ACVR1, AEBP2, AHDC1, ARID5B, ASCC3, ATP8B2, AXIN1, BMP7, C6orf201, CCDC6, CEP250, DKK1, DLL1, DNMT3B, EMSY, EPB41L5, EXT2, FGF8, FGFR1, FOXA1, FOXA2, HES7, HMGA2, HNF4A, HPRT1, HTT, KLF4, KLF5, LATS1, LEF1, LEFTY1, LEFTY2, MACF1, MBTD1, MEIS1, MIXL1, MTF2, NANOG, PBX3, PHF6, PITX2, POU5F1, PPP2CA, PRKAR1A, RARG, SESN1, SLC2A12, SMAD1, SOX17, SOX2, TBX1, TCF4, TEAD2, TET1, TOX3, TRERF1, TRIM71, TWSG1, UBR5, WDFY2, WNT3, WNT3A, ZIC2, ZIC5, ZNF281
All Shared	ACVR2A, AXIN2, BHLHE40, BMPR1A, BMPR2, C1QBP, CCND1, ELK4, EXT1, FOXC1, FOXH1, FZD8, JAK2, JARID2, RARB, SMAD3, SMAD4, SMAD6, SNAI1, SRF, TRIM28, VAV3, YAP1, ZFHX4
NC & Mesoderm Toxicants	ACVR2B, DDAH1, DIP2A, FZD5, GATA6, NABP2, PBX1, SMAD2

Figure 5 : mRNA targets specific to each toxicant group.
(A) Venn diagram overlapping the mRNA targets of up-regulated miRs for the GO Neural crest cell migration during development. (B) Venn diagram overlapping the mRNA targets of down-regulated miRs for the GO Mesodermal commitment pathway. (C) Table for the mRNAs in the Venn diagram in A. (D) Table for the mRNAs in the Venn diagram B. Full list of miRs that target the 66 mRNAs in B is available in Appendix Table 4.

MRNA Tab

Next, a bulk RNA-seq was performed from the same samples to obtain the differentially regulated mRNA within each treatment. The transcripts that are significantly differentiated within the NC and mesoderm toxicant groups can then be compared to the dysregulated miRs obtained in the analysis described above. This step will help infer the pattern of toxicant-induced gene regulation. We took the same approach as with the microRNA tab to first look at mRNAs overlapping all toxicants to identify the general toxicant induced differentially expressed mRNAs. Then the toxicants were separated into

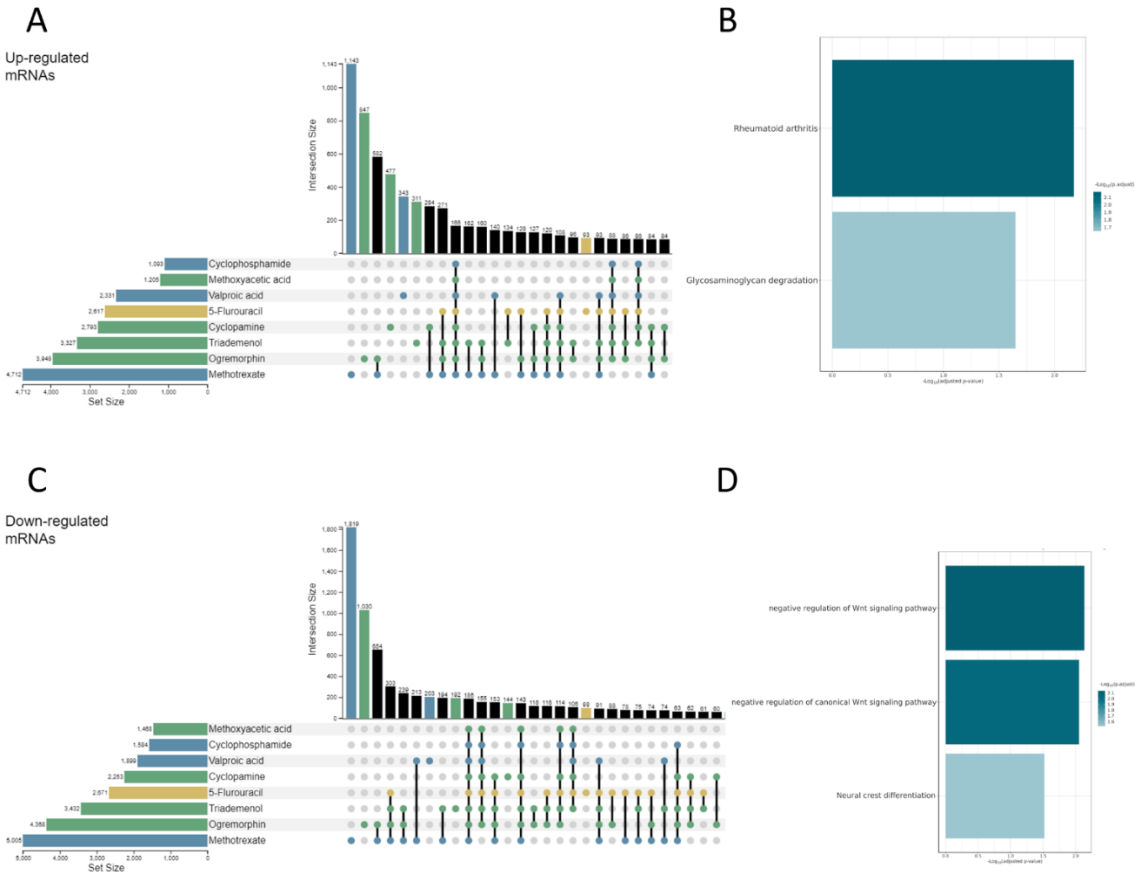

Figure 6 : Differentially expressed mRNAs overlapping all toxicants
(A) Upset plot overlapping all up-regulated mRNAs. (B) Gene ontologies for up-regulated mRNAs. (C) Upset plot overlapping all downregulated mRNAs. (D) Gene ontologies for downregulated mRNAs.

two subsets, one for the NC and the other for the mesoderm toxicants, to obtain specific lineage effects.

Within all toxicants a total of 166 mRNAs was differentially up-regulated (Fig. 6A). Six of these transcripts (*ATP6AP1, ATP6V0E2, ATP6V1G2, ATP6V1H, CTSL* and *TGFB3*) are involved with the GO rheumatoid arthritis. Three other mRNAs (*GLB1, HEXA,* and *SGSH*) associated within glycosaminoglycan degradation (Fig. 6B). Interestingly, glycosaminoglycans have been shown to promote osteogenic differentiation of human neural crest-derived cells and modifications of heparan sulfate, a glycosaminoglycan, affect human stem cell differentiation of mesoderm and endoderm lineages (Gasimli et al., 2014; Yanagisawa et al., 2022) validating our results Down-regulated mRNAs overlapping in all toxicants totaled 186 (Fig. 6C). Several of these down-regulated mRNAs (*EGR1, FRZB, GLI1, JADE1, SHISA3, SOX10, SOX2, TNN,* and *WIF1*) are annotated within Wnt pathways. Seven other down-regulated mRNAs (*CDH6, FGF19, MPZ, PAX3, PAX7, SOX10,* and *WNT1*) are annotated in the GO neural crest differentiation (Fig. 6D). This was an ideal result, as we observed up-regulated miRs with mRNA targets involved with neural crest cell migration. However, these down-regulated mRNAs were not the same as those listed in the MTI comparison in Figure 5A.

Next, to identify dysregulation specific to the sets of developmental toxicants , we separated the NC toxicants. There were 370 overlapping up-regulated mRNAs (Fig. 7A). Some of these mRNAs (*GLB1, GNS, HEXA,* and *SGSH*) are involved in glycosaminoglycan degradation pathways (Fig. 7B), similar to what we observed with all overlapping toxicants (Fig. 6B). In exclusively NC toxicants there were 24 overlapping

mRNAs, however, they did not produce gene ontologies in KEGG, Reactome or WikiPathways database. This may suggest that perturbations to glycosaminoglycan regulation is a result of pan-toxicity effects and not specific to NC toxicants. Yet, the number of identified transcripts was low, which often provides a challenge to associate a specific GO term.

A

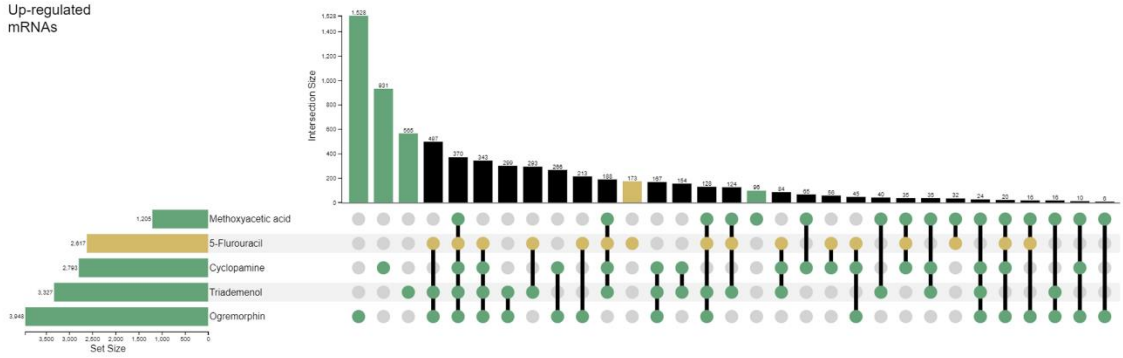

B

Description	p.adjust	geneID	Count
Lysosome	0.002114	ATP6AP1/ATP6V1H/CTSL/GLB1/GM2A/GNS/HEXA/MANBA/MCOLN1/SGSH/SMPD1/SORT1	12
Other glycan degradation	0.025231	GLB1/HEXA/MAN2B2/MANBA	4
Ether lipid metabolism	0.025231	GDPD3/PAFAH2/PEDS1/PLA2G2F/PLD3/PLPP3	6
Glycosaminoglycan degradation	0.025231	GLB1/GNS/HEXA/SGSH	4
Hippo signaling pathway	0.044419	AMOT/CDH1/FZD4/ID2/LLGL2/TGFB3/WNT5A/WNT6/WNT7B/WTIP	10

C

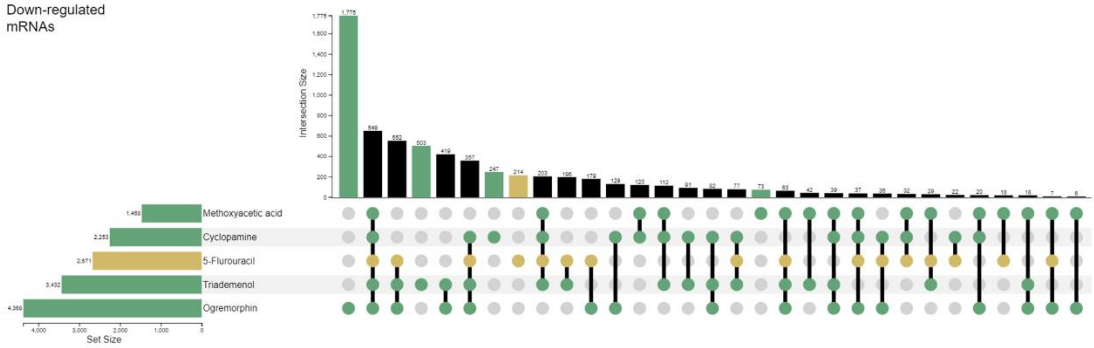

D

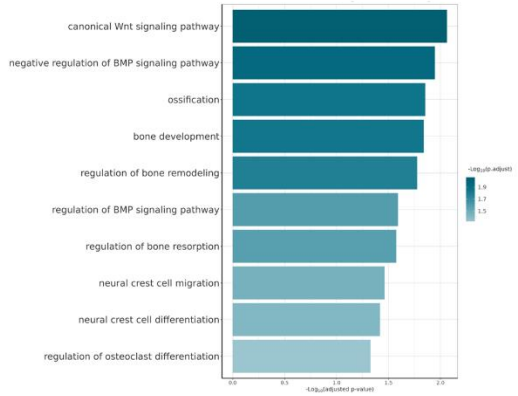

Figure 7 : Differentially expressed mRNAs overlapping neural crest toxicants.
(A) Upset plot overlapping all up-regulated mRNAs. (B) Gene ontologies for up-regulated mRNAs. (C) Upset plot overlapping all downregulated mRNAs. (D) Gene ontologies for downregulated mRNAs.

For down-regulated mRNAs in NC toxicants there was 649 mRNAs that overlapped (Fig. 7C). These mRNAs are annotated in GO such as neural crest cell migration and many bone developmental ontologies (Fig. 7D). In the GO neural crest cell migration there are seven down-regulated mRNAs (*FGF19, RET, SEMA3G, SEMA4A, SEMA5B, SOX10*, and *SOX8*). However, in exclusively NC toxicants there were 39 mRNAs, which collectively did not produce any GO annotations. Within those 39 mRNAs were a few genes involved with maintaining stem cells and pluripotency such as *POU5F1* (Oct4) *CDH22* (Cadherin 22) and *SNAI3* (Snail Family Transcriptional Repressor 3).

To specifically obtain transcripts dysregulated in toxicant-induced changes to the mesoderm lineage, the mRNAs of toxicants cyclophosphamide, methotrexate, valproic acid, and positive control 5-FU were compared. There were 342 up-regulated mRNAs (Fig. 8A). Some of these mRNAs *(GLB1, HEXA, IDUA,* and *SGSH*) are involved with similar gene ontologies seen in the NC toxicants (up-regulated mRNAs), such as glycosaminoglycan degradation (Fig. 8B). In exclusively mesoderm toxicants, there were 52 mRNAs (Fig. 8A). Collectively these mRNAs did not annotate to any gene ontologies. Some of these mRNAs however are characteristic to an oxidative stress response, which often associate with a toxicity response. For example, *SIRT3* (Sirtuin 3) is involved with removing reactive oxygen species and *PRDX2* (Peroxiredoxin 2) acts as an antioxidant protecting cells in oxidative stress (Kang et al., 1998; Schlicker et al., 2008).

In addition, 252 down-regulated mRNAs were identified overlapping all mesoderm toxicants (Fig. 8C). Some of these mRNAs *(EDNRA, FGF19, FRZB, MEF2C, SEMA3E, SEMA4A, SOX10,* and *SOX9*) seem to have additional roles in neural crest cell

differentiation (Fig. 8D), which may suggest that these mesoderm toxicants could have overlapping functions as neural crest toxicants as well.

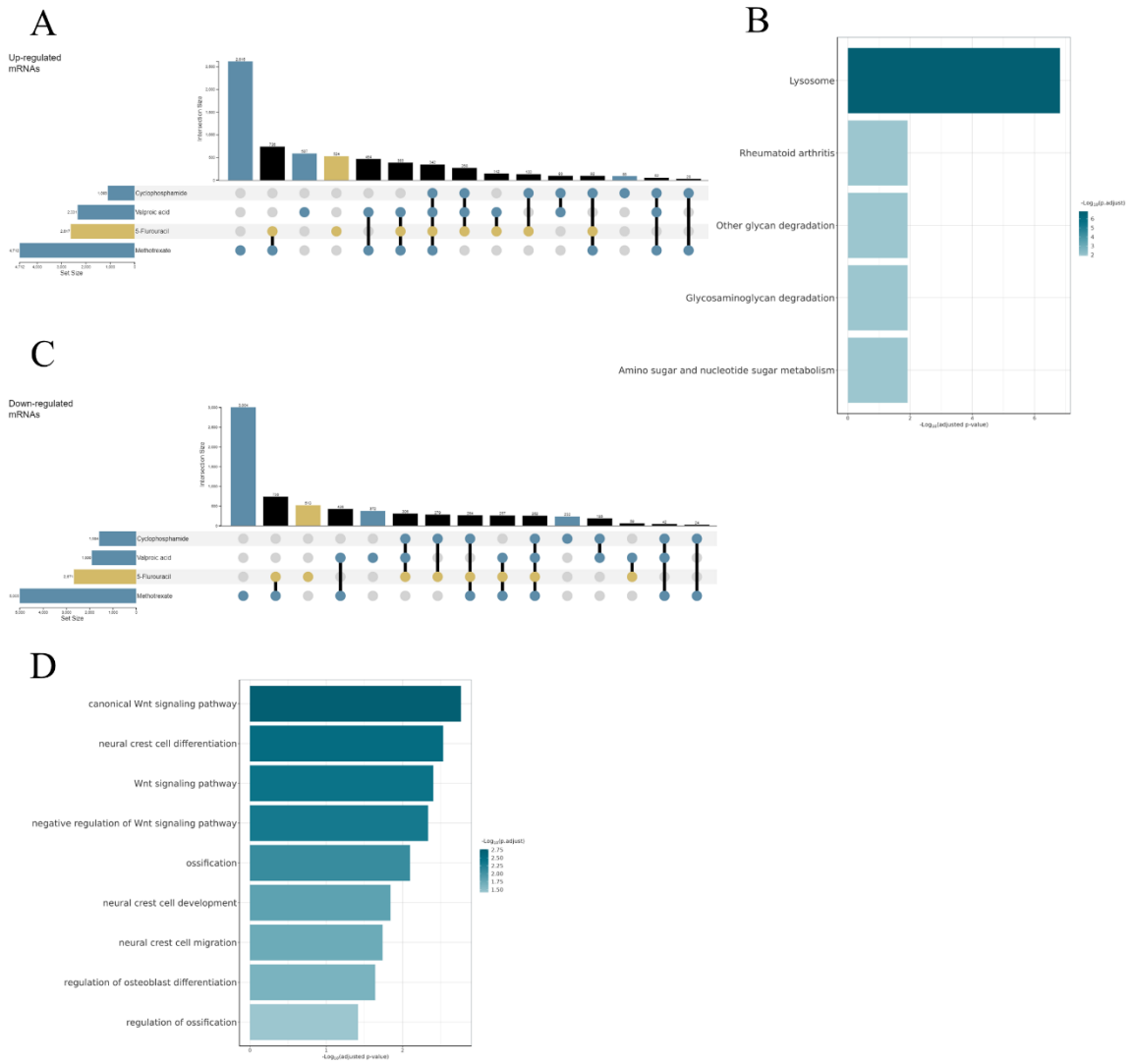

Figure 8 : Differentially expressed mRNAs overlapping mesoderm toxicants.
(A) Upset plot overlapping all up-regulated mRNAs. (B) Gene ontologies for 342 up-regulated mRNAs in upset plot. (C) Upset plot overlapping all downregulated mRNAs. (D) Gene ontologies for 252 downregulated mRNAs in upset plot.

Because GO neural crest differentiation was observed within the down-regulated mRNAs of NC-grouped and mesoderm-grouped toxicants, obtaining mRNAs specific to

each group may help us identify mRNAs specific to either the neural crest cell or the mesodermal lineage of bone differentiation. This can be done by comparing the mRNAs within the same GO of these toxicant groups. Below is a Venn diagram overlapping the down-regulated mRNAs within the GO neural crest differentiation (Fig. 9A). The mRNAs overlapping all, and those specific to NC, and mesoderm toxicants are listed in Fig. 9B. However, these mRNAs are not listed in the miRNA-target interactions (MTI) identified in the neural crest cell migration during development GO (Fig. 5C). However, some of the mRNAs (*AXIN2*, *FGFR1* and *ZIC5*) are targets in the mesodermal commitment pathway (Fig. 5D).

A

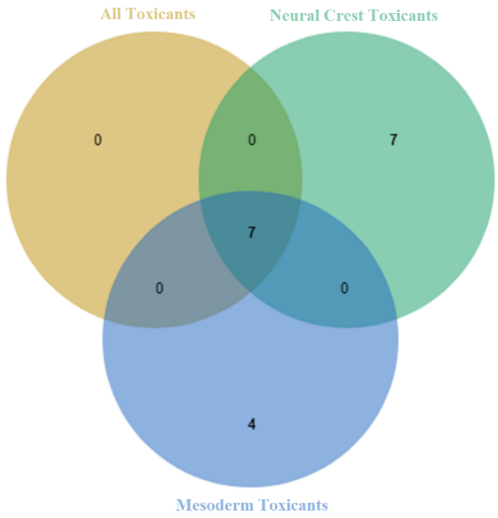

B

Neural crest differentiation	
Treatment	Down regulated mRNAs
Neural Crest Toxicants (7)	AXIN2, CDH2, FGFR1, FOXD3, LHX5, OLIG2, OLIG3
Mesoderm Toxicants (4)	FGF2, SOX5, SOX9, ZIC5
All Shared (7)	CDH6, FGF19, MPZ, PAX3, PAX7, SOX10, WNT1

Figure 9 : Overlapping downregulated mRNAs within GO neural crest differentiation.
A) Venn diagram displaying the number of overlapping mRNAs within each toxicant group. This includes positive control 5-FU. (B) Table displaying the mRNAs in the Venn diagram.

To search which miRs target the down-regulated mRNAs listed in Fig. 9B, the miRTox app can be used. By going to the miRNA expression tab, a table of the validated targets in up-regulated miRs can be generated. The table can then be searched for those down-regulated mRNAs to see if they are targets of any up-regulated miR. Table 3 below was generated with this approach. It displays the down-regulated mRNAs in Figure 9B that are targets of up-regulated miRs from the microRNA-seq.

Treatment	Up reg microRNA	Down reg mRNA
NC Toxicants	hsa-mir-34b-5p	AXIN2
Mesoderm Toxicants	hsa-mir-192-5p	FGF2
	hsa-mir-215-5p	FGF2
	hsa-mir-21-5p	SOX5
	hsa-mir-192-5p	ZIC5
	hsa-mir-215-5p	ZIC5

Table 3 : Up-regulated microRNAs targeting down-regulated mRNAs seen in GO neural crest differentiation.

The table above shows that these miRs may make suitable biomarkers within neural crest differentiation. However, a measure of the strength of the miR-mRNA relationship and whether it is statistically significant does not exist. To address this, another tab in the app to calculate the correlations and run hypothesis testing was incorporated.

Correlation Tab

This additional correlation tab aims to support observations identified in up-regulated miRs and their down-regulated targets (and vice versa) by calculating Pearson correlations between them. Significant pairs can be validated in the lab as potential biomarkers for developmental toxicity. This tab can be used in conjunction with a potential list of miR-mRNA pairs, such as the one in Table 3, by choosing the same toxicant groups, log2Fold-Change, false discovery rate and regulation. Alternatively, this tab could be used

alone to generate all miR-mRNA pairs, get gene ontologies, and see which pairs are significantly correlated. By following the same steps presented in the other tabs, overlapping all miRs within all toxicants, then subsetting to NC toxicants and mesoderm toxicants, potential miR-gene biomarkers can be obtained that show a significant correlated relationship.

MicroRNA-MRNA Pairs in all Toxicants

Within all toxicants 20 up-regulated miRs whose targets are also differentially down-regulated overlap in the upset plot (Fig. 10A). Without the positive control (5-FU) for pan-cellular toxicity, there are eight up-regulated miRs with down-regulated targets overlapping (Fig. 10A). Out of these eight miRs, five are significantly correlated miR-mRNA pairs (Fig. 10B). The pair hsa-mir-125b-1-3p – FRZB is of interest as *FRZB* is involved in regulating chondrocytes and in neural plate differentiation (Enomoto-Iwamoto et al., 2002; Williams et al., 2022; Yagi et al., 2022). In the toxicants cyclopamine, methoxyacetic acid, ogremorphin, triadimenol, cyclophosphamide, methotrexate and valproic acid, *DNMT3B* (DNA Methyltransferase 3 Beta) is negatively correlated with hsa-mir-148a-3p. DNMT3B establishes DNA methylation patterns during development and has been seen to be highly expressed in stem cells but diminished later during development (Liao et al., 2015; Rinaldi et al., 2016). Therefore, the up-regulation of mir-148a-3p may be one mechanism reducing levels of *DNMT3B*. These two pairs (miR-125b-1-FRZB and miR-148a-DNMT3B) show a moderate and strong correlation respectively. Their correlations are also significant as plotted in Figure 10C.

A

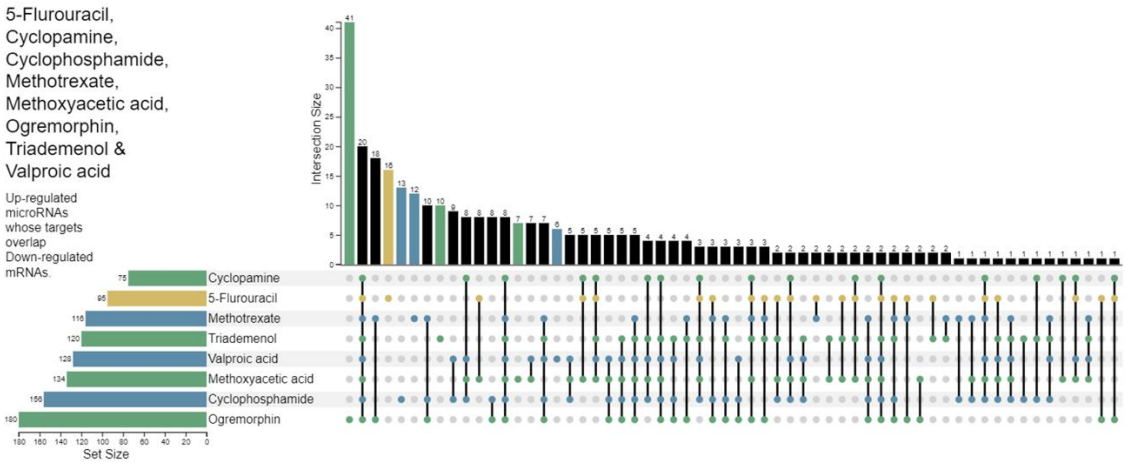

B

Overlap	microRNA	mRNA	Correlation	P-value
All Toxicants	hsa-mir-125b-1-3p	FRZB	-0.50	0.0127
	hsa-mir-21-5p	FKBP5	-0.45	0.0288
	hsa-mir-372-3p	CADM2	-0.40	0.0515
Cyclopamine, Methoxyacetic acid, Ogremorphin, Triademenol, Cyclophosphamide, Methotrexate & Valproic acid	hsa-mir-148a-3p	DNMT3B	-0.76	6.54439E-05
	hsa-mir-30a-5p	CAMKV	-0.53	0.0136

C

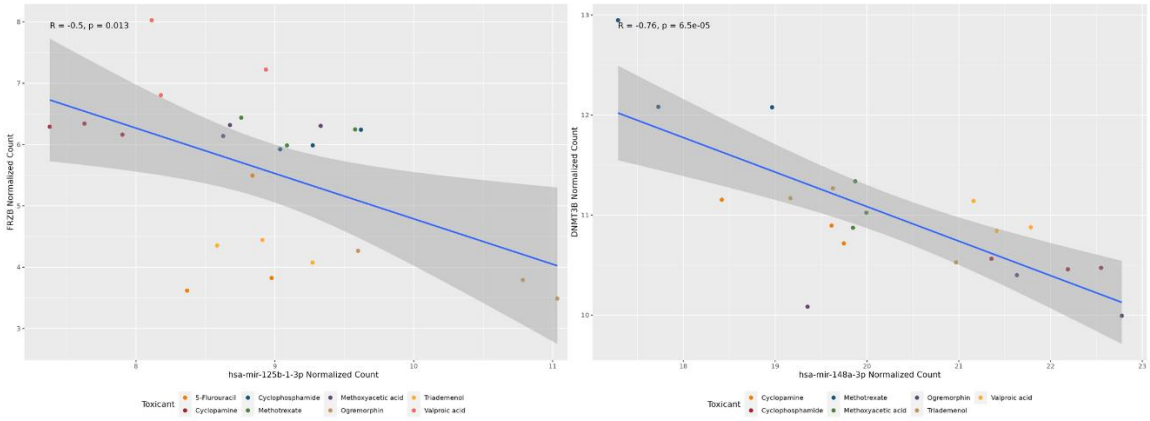

Figure 10 : Correlations of up-regulated miRs and downregulated mRNAs overlapping all toxicants
(A) Upset plot for miRs overlapping all toxicants and whose targets are downregulated. (B) Table showing the significantly negatively correlated miR-mRNA pairs. (C) Correlation plots for miR-125b-1-3-FRZB and miR-148a-DNMT3B pairs.

For down-regulated miRs and up-regulated mRNAs, there were 42 miRs overlapping all toxicants (Fig. 11A). Out of the 42 miRs, only 3 were significantly negatively correlated with an mRNA (Fig. 11B). In the overlap with cyclopamine, methoxyacetic acid, ogremorphin, triadimenol, cyclophosphamide, methotrexate and valproic acid, there were 5 miRs (Fig. 11A) and one of them was significantly negatively correlated with a mRNA (Fig. 11B). Two mRNAs were involved with promoting cell survival (*BCL2L2)* and double stranded break repair (*AP5Z1*, Adaptor Related Protein Complex 5 Subunit Zeta 1) (Fig. 11B).

A

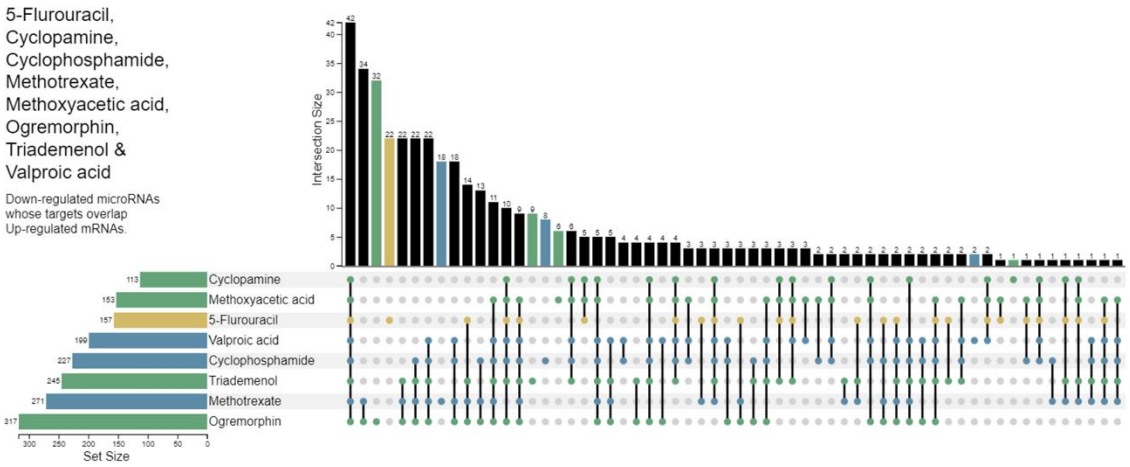

B

Overlapping	microRNA	mRNA	correlation	p_value
All	hsa-mir-1296-5p	SH3TC2	-0.690	0.000192
	hsa-mir-520a-3p	IRF2	-0.667	0.000369
	hsa-mir-520a-3p	LCP1	-0.656	0.000504
	hsa-mir-1296-5p	BCL2L2	-0.572	0.003493
	hsa-mir-106a-3p	PNRC1	-0.519	0.009338
	hsa-mir-520a-3p	BCL2L2	-0.469	0.020725
	hsa-mir-520a-3p	HS3ST1	-0.412	0.045304
Cyclopamine, Methoxyacetic acid, Ogremorphin, Triademenol, Cyclophosphamide, Methotrexate & Valproic acid	hsa-mir-195-5p	AP5Z1	-0.585	0.00534
	hsa-mir-195-5p	LURAP1L	-0.439	0.046287

Figure 11 : Correlations of downregulated miRs and up-regulated mRNAs overlapping all toxicants
(A) Upset plot for miRs overlapping all toxicants and whose targets are up-regulated. (B) Table showing the significantly negatively correlated miR-mRNA pairs.

MicroRNA-MRNA Pairs in Neural Crest Toxicants

For neural crest toxicant specific miR-mRNA correlated pairs, the NC toxicants were separated into a subset. Among these toxicants 25 miRs were up-regulated (Fig. 12A) and six of these were significantly negatively correlated with a mRNA (Fig. 12B). Among these pairs, *FRAT2*, *FRZB* and *TCF7* are involved in the Wnt signaling pathway and the

other mRNAs, *SOX2 and DNMT3B* are involved in stem cell differentiation. The hsa-mir-125b-1-3p – FRZB pair was previously observed in all toxicants (Fig. 10C) but among the NC toxicants it was more negatively correlated, -0.63. Among the NC-exclusive toxicants, N-cadherin (*CDH2*) was negatively correlated with mir-30a. Cadherins regulate neural crest cell migration during the epithelial-to-mesenchymal transition (Stepniak et al., 2009) validating our approach. It has been observed within chick embryos that these cadherins are carefully regulated during NC cell fate specification, to the point that the balance of the levels of cadherin expression can determine the specification of the NC cells to neural or non-neural tissues (Dady et al., 2012; Rogers et al., 2018). These miRs were up-regulated within NC toxicants and may down-regulate mRNAs required for proper cell differentiation. As for the down-regulated miRs that correlate with up-regulated mRNAs (Fig. 12C), there were the same pairs as observed in Fig. 11B. In NC toxicants, mir-520a-BCL2L2 was more negatively correlated (-0.81) but across all toxicants it was -0.47. Also, different miR pairs with *TFAP2A* (Transcription Factor AP-2 Alpha) was negatively correlated. *TFAP2A* is one of the neural plate border specifiers that also regulates neural crest specifier genes (Hockman et al., 2019; Simões-Costa & Bronner, 2015).

A

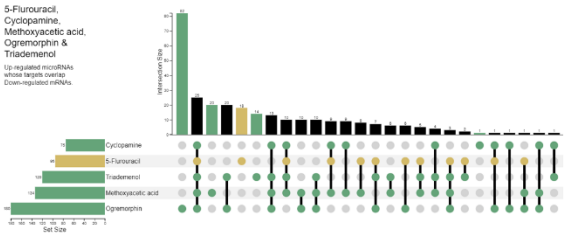

B

Toxicants	microRNA	Target	Correlation	P-value
All	hsa-mir-22-3p	FRAT2	-0.70	0.003892
	hsa-mir-29c-3p	FRAT2	-0.67	0.006199
	hsa-mir-125b-1-3p	FRZB	-0.63	0.011534
	hsa-mir-215-5p	TCF7	-0.50	0.057546
	hsa-mir-21-5p	SOX2	-0.62	0.014667
	hsa-mir-29c-3p	DNMT3B	-0.56	0.031537
	hsa-mir-143-3p	ADAMTS4	-0.85	4.95E-05
Cyclopamine Methoxyacetic acid Ogremorphin & Triademenol	hsa-mir-30a-5p	CDH2	-0.85	0.000401
	hsa-mir-148a-3p	DNMT3B	-0.65	0.021012

C

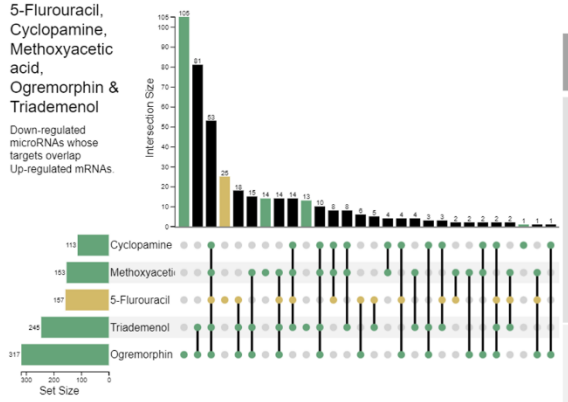

D

Toxicants	microRNA	Target	Correlation	P-value
All	hsa-mir-520a-3p	BCL2L2	-0.81	0.000227
	hsa-mir-1296-5p	BCL2L2	-0.67	0.006386
	hsa-mir-302d-5p	TFAP2A	-0.76	0.000986
	hsa-mir-302c-5p	TFAP2A	-0.76	0.001025
	hsa-mir-15b-5p	TFAP2A	-0.68	0.005157
Cyclopamine Methoxyacetic acid Ogremorphin & Triademenol	hsa-mir-195-5p	TFAP2A	-0.74	0.006458
	hsa-mir-195-5p	BCL2L2	-0.70	0.011203

Figure 12 : Correlations of miR-mRNA pairs within NC toxicants
(A) Upset plot for up-regulated miRs whose targets are downregulated. (B) Significant correlations for miRs in A overlapping all and without 5-FU for the miR-mRNA pairs. (C) Upset plot for downregulated miRs whose targets are up-regulated. (D) Significant correlations for miRs in C within all overlapping and without 5-FU.

To isolate mesoderm-specific miR-mRNA pairs subsetting the mesoderm toxicants when the miR was up-regulated and its targets down-regulated identified 21 overlapping miRs (Fig. 13A). Within these miRs only one pair was significantly correlated: miR-192-SGMS2 (Fig. 13B). In human subjects, single nucleotide polymorphisms (SNPs) within the *SGMS2* (Sphingomyelin Synthase 2) gene are associated with cranial sclerosis and defects in bone

mineralization (Pekkinen et al., 2019). While this was observed in mature bone tissue , this gene may also play a role in the mineralization of differentiating cells. Within mesoderm exclusive toxicants (cyclophosphamide, methotrexate & valproic acid), two miR pair with mRNAs *DNMT3B* and *JARID2* (Jumonji And AT-Rich Interaction Domain Containing 2) were observed to be significantly negatively correlated (Fig. 13B). These two mRNAs were observed to be down-regulated in stem cells and are required to be up-regulated during differentiation to mesoderm (Pasini et al., 2010; Yu et al., 2017). These data confirm that cyclophosphamide, methotrexate and valproic acid interfere with mesoderm differentiation.

A

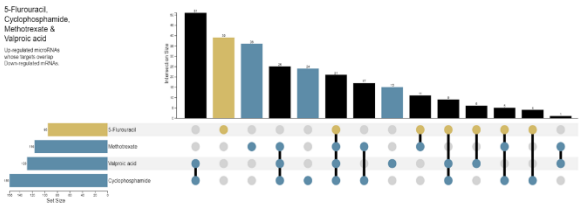

B

Toxicant	microRNA	Target	Correlation	P-value
ALL	hsa-mir-192-5p	SGMS2	-0.63	0.029551
Cyclophosphamide, Methotrexate & Valproic acid	hsa-mir-148a-3p	DNMT3B	-0.96	2.62E-05
	hsa-mir-148a-3p	JARID2	-0.70	0.036866
	hsa-mir-7-5p	JARID2	-0.67	0.0472

C

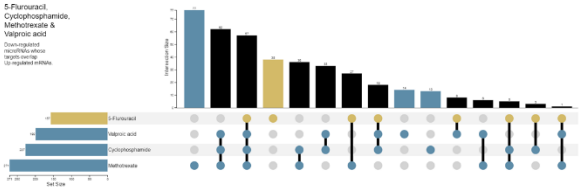

D

Toxicant	microRNA	Target	Correlation	P-value
All	hsa-mir-329-3p	VANGL1	-0.64	0.023946
	hsa-mir-520a-3p	IRF2	-0.85	0.000435
Cyclophosphamide, Methotrexate & Valproic acid	hsa-mir-20a-3p	VANGL1	-0.68	0.044246
	hsa-mir-519a-3p	IRF2	-0.86	0.003251
	hsa-mir-519b-3p	IRF2	-0.84	0.004483

Figure 13 : Correlations of miR-mRNA pairs within mesoderm toxicants
(A) Upset plot for up-regulated miRs whose targets are downregulated. (B) Significant correlations for miRs in A overlapping all and without 5-FU for the miR-mRNA pairs. (C) Upset plot for downregulated miRs whose targets are up-regulated. (D) Significant correlations for miRs in C within all overlapping and without 5-FU.

Overlapping down-regulated miRs and up-regulated mRNAs (Fig. 13C) produced significant pairs of miRs with two mRNAs, *VANGL1* and *IRF2*. The Wnt-planar cell

polarity gene *VANGL1* (VANGL Planar Cell Polarity Protein 1) mainly regulates gastrulation and neural tube closure (M. Wang et al., 2019). In neural crest cells, that *VANGL1* is not required for NC migration but instead identifies as a neural crest specifier gene (Deichmann et al., 2015; Pryor et al., 2014). The other mRNA *IRF2* was highly negatively correlated with miR-520a and miR-519a and 519b. While*IRF2* has not yet been identified to regulate mesoderm or neural crest differentiation, its cousin *Irf6* has recently been implicated in the control of midface development in mice (Carroll et al., 2020). It also contributed to facial clefting in humans (Ghassibe-Sabbagh et al., 2021), underlining the value of the developed app in the identification of known and novel miR-mRNA interactions.

Conclusion

By developing this app, microRNA and mRNA datasets were individually analyzed and both microRNAs and mRNAs that are specific to neural crest and mesoderm differentiation were obtained. By incorporating a 'Correlation Analysis' tab the number of mRNAs from were reduced from hundreds to a few dozen by comparing them to the validated microRNA targets generated from the miRNA sequencing. However, pairs of miRNA-target interactions selected from overlapping gene ontologies were not significantly negatively correlated. Therefore, to find pairs of miRNA-mRNA that were significantly correlated, the app provided a valuable tool to easily combine miRNAs from one sequencing, obtain the validated targets, intersect them with differentially expressed mRNAs from another sequencing and calculate correlations. This process would have been tedious to perform in other manual approaches, such as using excel. Any user regardless of coding skill level

would be able to use the app and quickly generate figures and results. Through this process a few potential biomarkers were selected. For neural crest toxicity they were miR-30a-*CDH2*, miR-148a-*DNMT3B* and miR-195-*TFAP2A*. Potential biomarkers identified for mesoderm toxicity were miR-148a-*DNMT3B/JARID2* and miR-7-*JARID2*.

Appendix

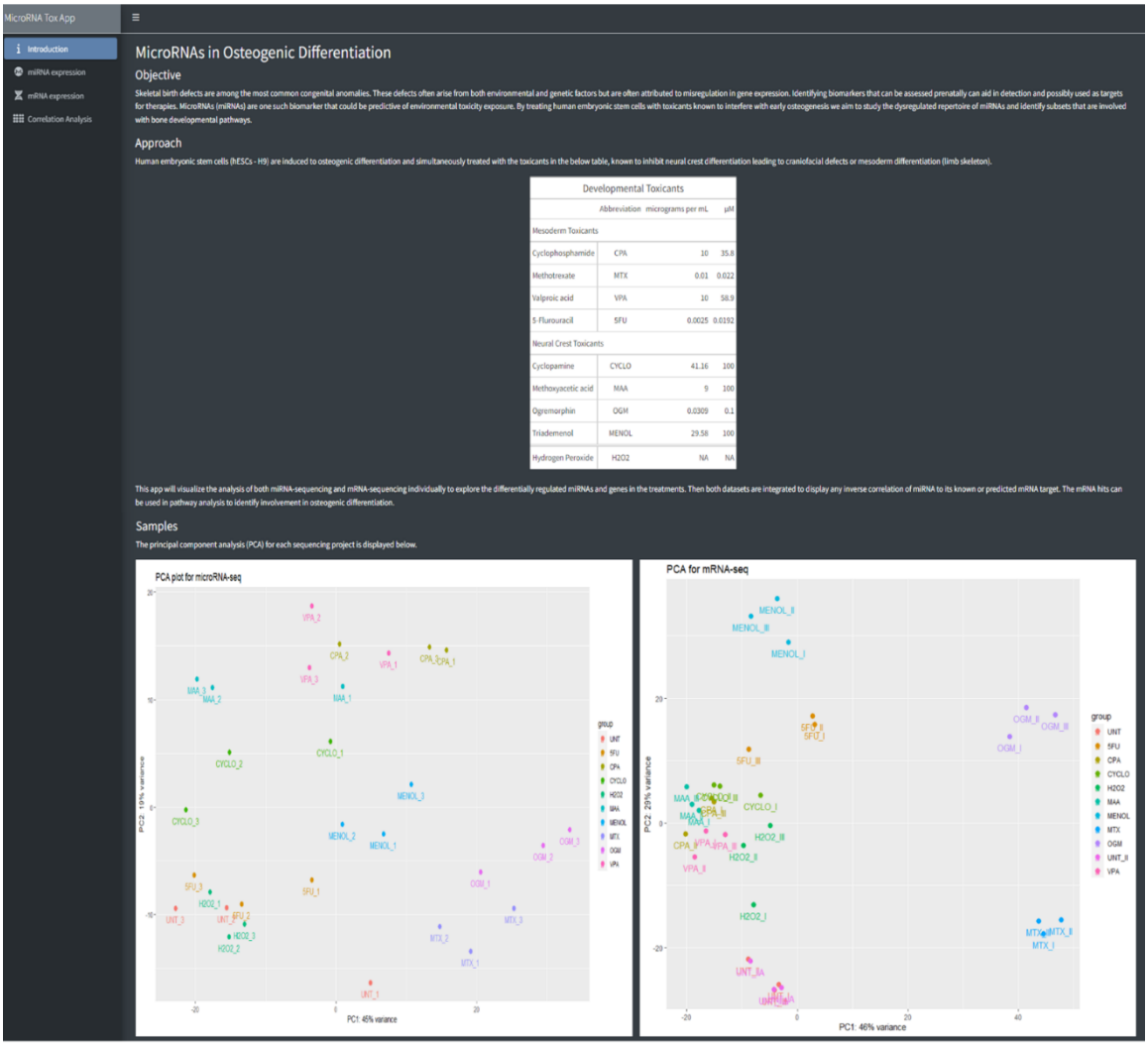

Appendix Figure 1: Introduction section of microRNA Tox app

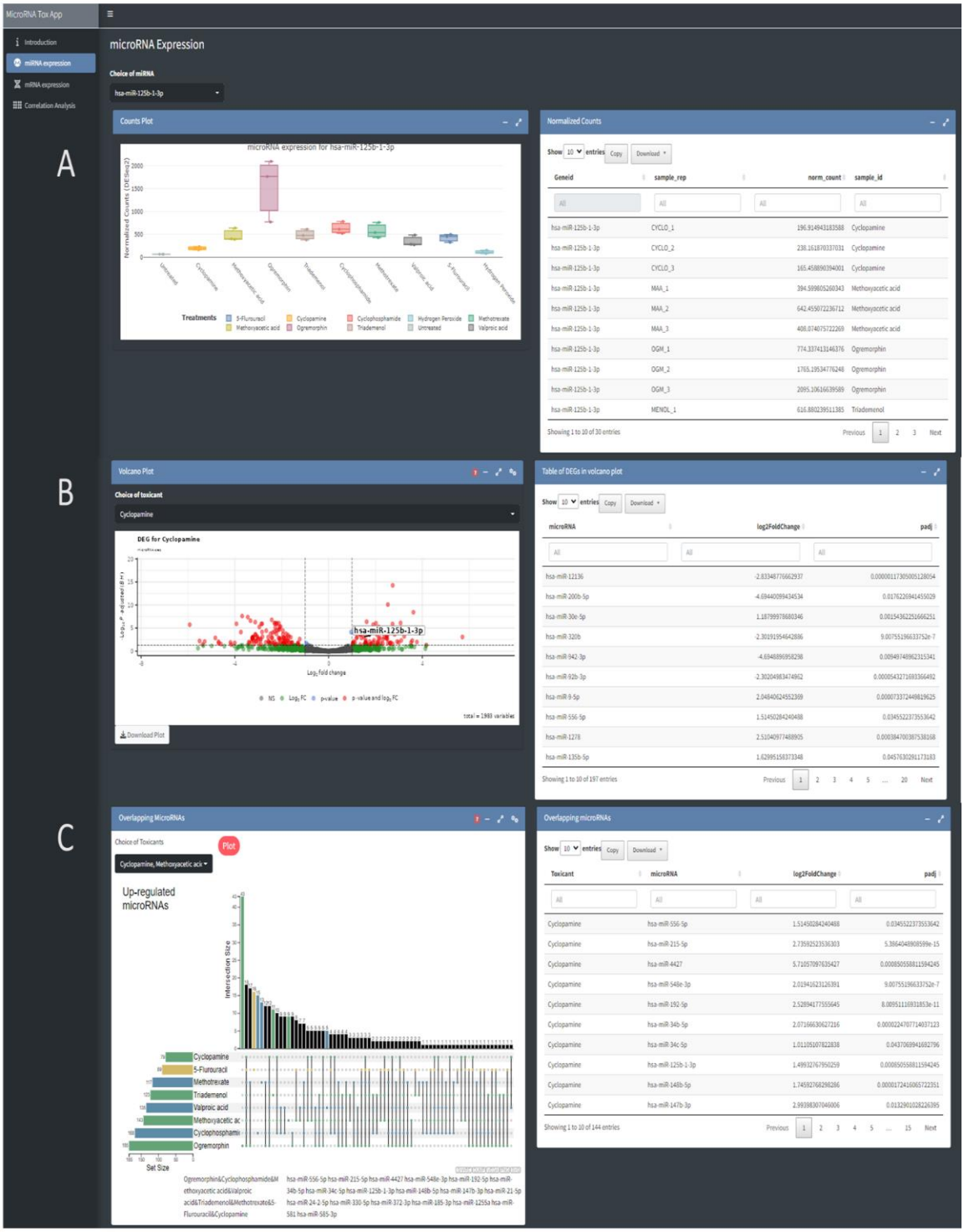

Appendix Figure 2 : MicroRNA section of microRNA Tox app

(A) Boxplots of normalized counts for selected miR with counts in adjacent table. (B) Volcano plot of the differential expression for selected toxicant with adjacent table displaying the values for the red dots in volcano plot. (C) Upset plot for selected toxicants with adjacent table displaying the selected intersections in the upset plot.

Appendix Figure 3 : MicroRNA section of microRNA Tox app

(A) Heatmap for selected toxicants with three options in tabs to generate a heatmap for all replicates, median of replicates or select miRs. (B) Radar plot with choice in two tabs to display select miRs and overlay the log2foldchange within the toxicants or to display select toxicants and overlay the miR.

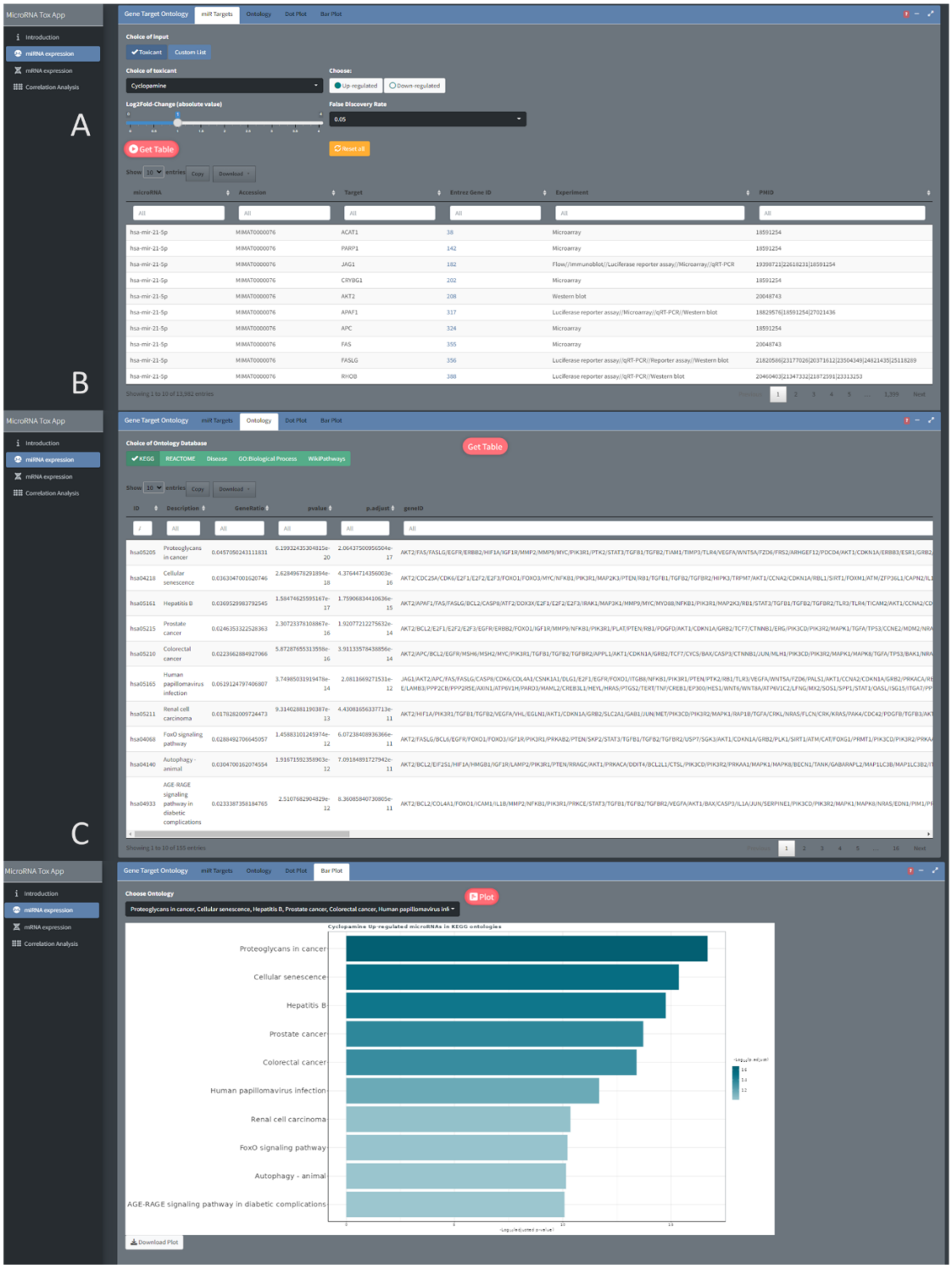

Appendix Figure 4 : Gene target ontology in section microRNA expression

(A) Table of miR targets within selected toxicant or choice to input a custom list of miRs. (B) Ontology tab displaying choice of GO database and table of GO terms generated from the miR targets in first tab.(C) Bar plot tab generates plot for user selected GO terms generated in Ontology tab.

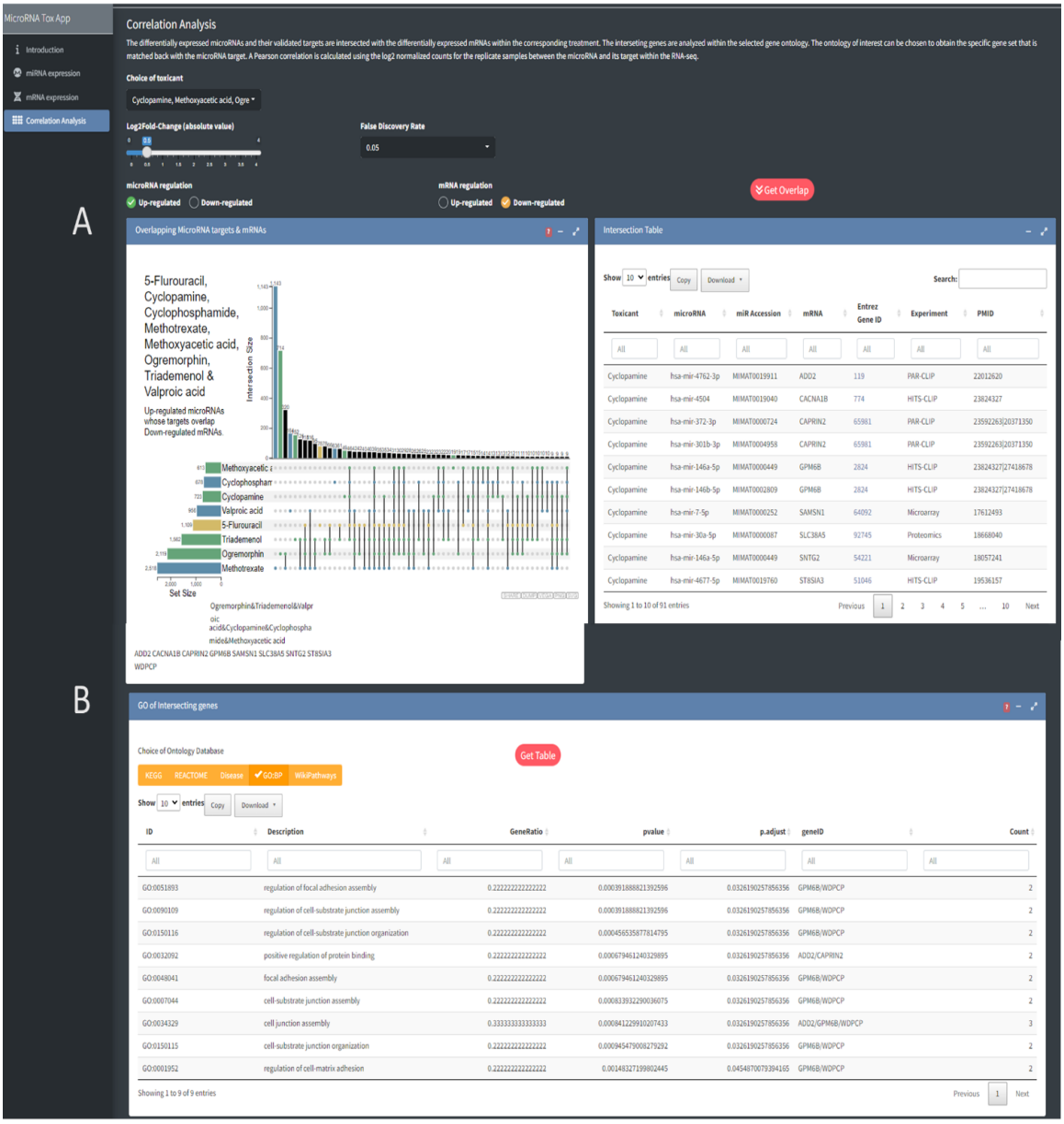

Appendix Figure 5 : Correlation analysis section of microRNA tox app

(A) Upset plot for user selected toxicants with options to adjust log2foldchange, false discovery rate (p-value) and direction of differential expression (up or down-regulated). The adjacent table displays the miR and its target mRNA selected from the overlap column in the upset plot.(B) Table of GO terms from a choice of five databases. GOs are generated from the mRNAs in the upset plot table.

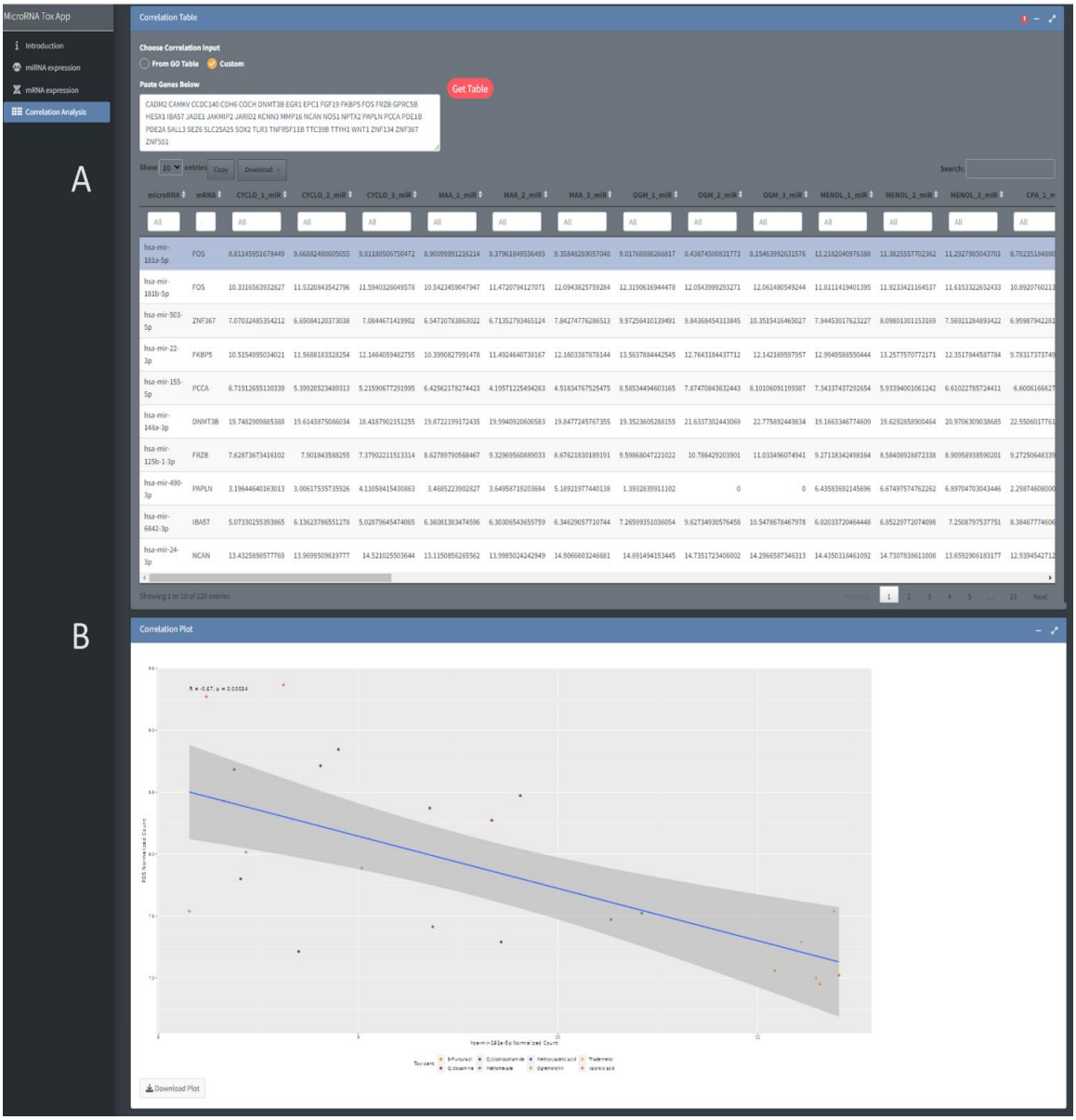

Appendix Figure 6 : miR-mRNA correlations in section correlation analysis

(A) Table of miR-mRNA Pearson correlations among toxicants chosen initially in correlation analysis section. User has a choice to generate correlation from the GO terms generated in this section or enter a list of mRNAs from overlaps in the upset plot in this section. (B) Correlation plot for the selected row in the correlation table.

	microRNA	Target
Mesodermal commitment pathway	hsa-mir-125b-1-3p	BMPR2
	hsa-mir-143-3p	HNF4A, KLF5, SMAD3, TRIM71
	hsa-mir-185-3p	PPP2CA, VAV3
	hsa-mir-192-5p	ACVR2A, ACVR2B, BCORL1, BMPR2, FOXA1, FZD4, MACF1, NLK, PHF6, PRKAR1A, WDCP, WNT3, ZIC5
	hsa-mir-21-5p	BMPR2, DDAH1, KLF5, LATS1, MEIS1, PBX1, SESN1, SETD2, SOX2, TET1, UBR5
	hsa-mir-215-5p	ACVR2B, BMPR2, FOXA1, FZD4, MACF1, NLK, PHF6, PRKAR1A, WDCP, WNT3, ZIC5
	hsa-mir-24-2-5p	PRKAR1A
	hsa-mir-30e-5p	DDAH1, FOXA1, MTF2, PRKAR1A, SNAI1, WDFY2
	hsa-mir-330-5p	BMP7, CCND1, HMGA2, ZNF462
	hsa-mir-34b-5p	AXIN2, HNF4A
	hsa-mir-34c-5p	CCND1, HNF4A, JARID2, NANOG, RARG, SMAD4, SNAI1, SOX2, VAV3
	hsa-mir-372-3p	CCDC6, DKK1, ELK4, GATA6, LEFTY1, MIXL1
	hsa-mir-455-5p	VAV3
	hsa-mir-548e-3p	ACVR2B, LEFTY1
	hsa-mir-556-5p	CCND1

	microRNA	Target
Neural crest cell migration during development	hsa-mir-148a-3p	STAT3
	hsa-mir-30a-5p	BDNF,JUN,PIK3CD,TRIO
	hsa-mir-7-5p	AKT3,FOS,PAK1,PIK3CB,PIK3CD,PIK3CG,PIK3R3

Appendix Table 1 : Up-regulated miRNAs validated targets in all toxicants

Top: Up-regulated miRNAs in all overlapping toxicants involved with validated targets annotated in GOs mesodermal commitment pathway. Bottom: neural crest cell migration during development.

Database	ID	Description	p.adjust	geneID	Count
WikiPathways	WP2857	Mesodermal commitment pathway	0.004412	BMPR2/KLF5/MEIS1/PBX1/SOX2/LATS1/DDAH1/SESN1/SETD2/UBR5/TET1/ACVR2A/ACVR2B/FOXA1/PRKAR1A/WNT3/FZD4/MACF1/NLK/BCORL1/WDCP/PHF6/ZIC5/HNF4A/SMAD3/TRIM71/AXIN2/CCND1/JARID2/SMAD4/RARG/SNAI1/VAV3/NANOG/MTF2/WDFY2/ELK4/GATA6/CCDC6/LEFTY1/DKK1/MIXL1/PPP2CA/BMP7/HMGA2/ZNF462	46
WikiPathways	WP474	Endochondral ossification	0.002166	IGF1R/MEF2C/MMP9/DDR2/PLAT/SOX5/TGFB1/TGFB2/TIMP3/VEGFA/AKT1/FGF2/HMGCS1/PLAU/MMP13/ADAMTS4/RUNX2/ADAMTS1/FRZB/THRA/BMP7/IHH/CALM1/SCIN	24
WikiPathways	WP4808	Endochondral ossification with skeletal dysplasias	0.002166	IGF1R/MEF2C/MMP9/DDR2/PLAT/SOX5/TGFB1/TGFB2/TIMP3/VEGFA/AKT1/FGF2/HMGCS1/PLAU/MMP13/ADAMTS4/RUNX2/ADAMTS1/FRZB/THRA/BMP7/IHH/CALM1/SCIN	24
WikiPathways	WP1434	Osteopontin signaling	0.00526	MMP9/NFKB1/ITGAV/ITGB3/PLAU/MAPK1/MAP2K1/RELA	8
WikiPathways	WP322	Osteoblast signaling	0.00824	TNFRSF11B/BGLAP/ITGAV/ITGB3/COL1A1/PDGFB/PDGFRA/PDGFRB	8
WikiPathways	WP399	Wnt signaling pathway and pluripotency	8.03E-05	APC/LRP6/MYC/PRKCE/SOX2/WNT5A/FZD6/NFYA/PAFAH1B1/PLAU/MAPK9/TCF7/WNT3/FZD1/FZD4/FZD7/ZBTB33/FBXW2/PPP2R3B/RACGAP1/NLK/CD44/CTNND1/PPP2R2A/PPP2R5E/MAP3K7/CTNNB1/AXIN2/CCND1/FOSL1/NANOG/LDLR/PPP2R1B/TP53/CCND2/FZD9/PRKCA/PPP2CA/PTPA	39
WikiPathways	WP428	Wnt signaling	0.016793	APC/CSNK1A1/LRP6/MYC/WNT5A/FZD6/DAAM1/PRICKLE2/GPC4/PLAU/MAPK9/TCF7/WNT3/FZD1/FZD7/NLK/CTNNBIP1/VANGL1/PRICKLE1/NFATC1/MAP3K7/CTNNB1/CCND1/FOSL1/PPP3CB/MAPK8/ROCK2/KREMEN1/CCND2/FZD9/DKK1/PRKCA/SENP2/FRAT2	34

Database	ID	Description	p.adjust	geneID	Count
WikiPathways	WP4565	Neural crest cell migration in cancer	0.010144	BDNF/JUN/PIK3CD/TRIO/KIDINS220/STAT3/FOS/PAK1/PIK3CB/PIK3CG/PIK3R3/AKT3	12
WikiPathways	WP4564	Neural crest cell migration during development	0.016598	BDNF/JUN/PIK3CD/TRIO/STAT3/FOS/PAK1/PIK3CB/PIK3CG/PIK3R3/AKT3	11
WikiPathways	WP399	Wnt signaling pathway and pluripotency	0.004161	CD44/CTNNB1/CTNND1/JUN/LDLR/PPP2R1B/PPP2R2A/PTPA/PPP2R5C/TP53/WNT5A/APC/MMP7/MYC/PPARD/WNT1/WNT10B/WNT2B/FZD5/LRP6/NFYA/MAPK9/NKD1	23
WikiPathways	WP428	Wnt signaling	0.015947	CTNNB1/JUN/PPP3CA/PPP3CB/PPP3R1/MAPK8/WNT5A/ROCK2/KREMEN1/APC/CSNK2A1/MYC/WNT1/WNT10B/WNT2B/FZD5/SENP2/CAMK2D/LRP6/ROR1/MAPK9/RYK/NKD1	23
WikiPathways	WP4787	Osteoblast differentiation and related diseases	0.011976	RUNX2/CTNNB1/SMAD1/NOTCH1/PIK3C2B/PIK3CD/PIK3R2/MAPK1/MAPK8/WNT5A/WNT1/WNT10B/WNT2B/FZD5/BMPR2/FGF1/RBPJ/LRP6/PIK3CB/PIK3CG/MAPK9/WNT8B/PIK3R3/BMPR1A	24

Appendix Table 2 : GO table for up-regulated miRNAs in all toxicants

Top: Table of GOs in figure 1B. Bottom: Table of GOs in figure 1C.

Database	ID	Description	p.adjust	geneID	Count
WikiPathways	WP4564	Neural crest cell migration during development	0.011957	BDNF/MMP9/PAK2/AKT3/PAK4/RAC1/TWIST1/AKT1/EPHB1/F2RL2/PIK3R3/ARF1/PIK3CD/TRIO/STAT3/PIK3CB/EPHB2/PAK3/RHOA/AKT2	20
WikiPathways	WP2857	Mesodermal commitment pathway	0.013164	BMPR1A/FOXC1/JAK2/JARID2/SMAD4/SMAD6/MEIS1/PRKAR1A/SNAI1/TCF4/HMGA2/FZD8/VAV3/ACVR2A/CCND1/ELK4/EXT1/SMAD2/SMAD3/RARB/AXIN2/BHLHE40/ZFHX4/KLF5/POU5F1/SOX2/KLF4/PARP8/NANOG/MIXL1/ACVR1/PAX6/PRKACA/ACACA/CTBP2/MTF2/PPP2CA/GATA6/CCDC6/LEFTY1/KDM6A/FZD5/SRF/DDAH1/ATP8B2/BMPR2/NLK/NCAPG2/NABP2/ZIC5/ADAM19/WDFY2/TEAD1/FZD4/ARID5B/RARG/AXIN1/ZNF281/TBX1	59
WikiPathways	WP474	Endochondral ossification	0.027503	ALPL/BMPR1A/RUNX2/MMP9/PLAT/FGF2/TGFB1/THRA/VEGFA/IGF1R/SOX9/STAT1/TGFB2/AKT1/PRKACA/CALM1/DDR2/IHH/STAT5B/CAB39/SLC38A2/CDKN1C/IGF1/KIF3A/IGF2/SCIN/ADAMTS1	27
WikiPathways	WP4808	Endochondral ossification with skeletal dysplasias	0.027503	ALPL/BMPR1A/RUNX2/MMP9/PLAT/FGF2/TGFB1/THRA/VEGFA/IGF1R/SOX9/STAT1/TGFB2/AKT1/PRKACA/CALM1/DDR2/IHH/STAT5B/CAB39/SLC38A2/CDKN1C/IGF1/KIF3A/IGF2/SCIN/ADAMTS1	27
WikiPathways	WP1425	Bone morphogenic protein signaling and regulation	0.023756	BMPR1A/RUNX2/SMAD4/SMAD6/TOB2/SMURF1/BMPR2/TOB1	8
WikiPathways	WP399	Wnt signaling pathway and pluripotency	9.19E-05	CD44/DVL3/TCF7L2/FZD1/FZD8/RACGAP1/CCND1/CCND2/CCND3/CSNK1E/GSK3B/PAFAH1B1/PPP2R5C/PRKCD/MAP2K4/MAP3K7/AXIN2/FZD6/FZD9/ZBTB33/CTNND1/MYC/POU5F1/SOX2/FZD7/NANOG/PPP2R5E/CREBBP/CTBP2/DVL1/PPP2CA/WNT5A/FZD5/LDLR/FBXW2/NLK/FZD2/EP300/LRP6/PPP2CB/PRKCB/CTNNB1/NFYA/WNT7B/PPP2R2A/FZD4/WNT16/RHOA/AXIN1/FOSL1	50
WikiPathways	WP363	Wnt signaling pathway	0.006127	DVL3/TCF4/TCF7L2/PI4K2A/CCND1/CDK6/CSNK1E/GSK3B/MAPK1/MAP3K7/TCF3/AXIN2/MYC/RAC1/AKT1/DVL1/CSNK1A1/NFATC2/TSC1/NLK/LRP6/PRKCB/CTNNB1/RHOA/AXIN1	25

Database	ID	Description	p.adjust	geneID	Count
WikiPathways	WP2857	Mesodermal commitment pathway	0.018041	CCND1/BMPR1A/FOXC1/SMAD6/SNAI1/FZD8/VAV3/ACVR2A/ELK4/EXT1/JAK2/JARID2/SMAD3/RARB/AXIN2/BHLHE40/YAP1/ZFHX4/SMAD4/SRF/BMPR2/C1QBP/FOXH1/TRIM28	24
WikiPathways	WP1434	Osteopontin signaling	0.019588	MMP9/MAP2K1/CHUK/MAPK1/MAPK3	5
WikiPathways	WP4787	Osteoblast differentiation and related diseases	0.029725	BMPR1A/NOTCH1/FZD8/RUNX2/FGF2/FGFR4/RBPJ/NOTCH2/PIK3R1/PRKCD/WNT7A/FZD6/FZD9/FGF9/SMAD4/PIK3C2B/MAPK1/MAPK3/BMPR2	19
WikiPathways	WP399	Wnt signaling pathway and pluripotency	0.004048	CCND1/CD44/TCF7L2/FZD8/RACGAP1/CCND2/CCND3/CSNK1E/GSK3B/PAFAH1B1/PPP2R5C/PRKCD/MAP3K7/WNT7A/AXIN2/FZD6/FZD9/ZBTB33/NKD1/RHOA	20
WikiPathways	WP363	Wnt signaling pathway	0.008146	CCND1/CDK6/TCF7L2/PI4K2A/CSNK1E/GSK3B/MAP3K7/TCF3/AXIN2/RHOA/RAC1/MAPK1	12
WikiPathways	WP1425	Bone morphogenic protein signaling and regulation	0.000376	BMPR1A/SMAD6/RUNX2/TOB2/SMURF1/SMAD4/BMPR2	7

Appendix Table 3 : GOs for down-regulated miRNAs in all toxicants

Top: Table of GOs for plot in figure 2B. Bottom: Table of GOs for plot in figure 2C.

Target	Down-regulated microRNA	PMID
ACACA	hsa-mir-335-5p, hsa-mir-193b-3p, hsa-mir-520c-5p, hsa-mir-518d-5p	18185580, 23622248, 26701625, 26701625
ACVR1	hsa-mir-19b-3p, hsa-mir-335-5p, hsa-mir-454-3p	20371350, 18185580, 21572407
AEBP2	hsa-mir-484	23622248
AHDC1	hsa-mir-19a-3p, hsa-mir-19b-3p, hsa-mir-484, hsa-mir-193b-3p	22473208, 22473208, 23622248, 23622248
ARID5B	hsa-mir-767-3p, hsa-mir-4429	23592263, 23592263
ASCC3	hsa-mir-16-5p, hsa-mir-425-5p	18668040, 23622248
ATP8B2	hsa-mir-335-5p	18185580
AXIN1	hsa-mir-335-5p, hsa-mir-484	18185580, 23622248
BMP7	hsa-mir-34a-5p	23226240
C6orf201	hsa-mir-335-5p	18185580
CCDC6	hsa-mir-17-5p, hsa-mir-93-5p, hsa-mir-106a-5p, hsa-mir-302d-3p, hsa-mir-20b-5p, hsa-mir-519d-3p, hsa-mir-520d-3p	20371350, 20371350, 20371350, 20371350, 20371350, 20371350, 20371350
CEP250	hsa-mir-484	23622248
DKK1	hsa-mir-335-5p, hsa-mir-501-5p	26986081, 27846906
DLL1	hsa-mir-34a-5p, hsa-mir-335-5p	14697198|19461653|20144220|23327670, 18185580
DNMT3B	hsa-mir-93-5p, hsa-mir-335-5p	23622248, 18185580

Target	Down-regulated microRNA	PMID
EMSY	hsa-mir-17-5p, hsa-mir-93-5p, hsa-mir-106a-5p, hsa-mir-20b-5p, hsa-mir-519c-3p, hsa-mir-519b-3p, hsa-mir-519d-3p, hsa-mir-519a-3p	22473208|24398324|22012620|21572407|20371350, 22473208|24398324|22012620|21572407|20371350, 24398324|22012620|21572407|20371350, 22473208|24398324|22012620|21572407|20371350, 23592263|24398324|22012620|21572407|20371350, 23592263|24398324|22012620|21572407|20371350, 22473208|24398324|22012620|21572407|20371350, 23592263|24398324|22012620|21572407|20371350
EPB41L5	hsa-mir-17-5p	23622248
EXT2	hsa-mir-34a-5p	23622248
FGF8	hsa-mir-335-5p	18185580
FGFR1	hsa-mir-16-5p, hsa-mir-149-5p, hsa-mir-133b, hsa-mir-4485-5p	21885851, 24463821, 23296701, 23824327
FOXA1	hsa-mir-93-5p, hsa-mir-30c-5p, hsa-mir-625-5p	27829043, 21572407|27292025, 27292025
FOXA2	hsa-mir-335-5p	18185580|24449834
HES7	hsa-mir-605-5p, hsa-mir-766-3p	23446348|21572407|20371350|23706177|26701625|27292025, 23446348|21572407|20371350|23706177|27292025
HMGA2	hsa-mir-15a-5p, hsa-mir-16-5p, hsa-mir-106a-5p, hsa-mir-34a-5p	22139073, 22139073, 27383537, 19461653
HNF4A	hsa-mir-34a-5p, hsa-mir-766-3p	20018894|22232426|23298640|27135744, 22232426
HPRT1	hsa-mir-19a-3p, hsa-mir-19b-3p, hsa-mir-30c-5p, hsa-mir-34a-5p, hsa-mir-193b-3p, hsa-mir-454-3p	20371350, 20371350, 23622248, 19696787, 20304954, 20371350
HTT	hsa-mir-16-5p, hsa-mir-17-5p	23622248, 23622248
KLF4	hsa-mir-15a-5p, hsa-mir-34a-5p, hsa-mir-335-5p	23867820, 24415058|25362853|28250026, 18185580
KLF5	hsa-mir-489-3p	22100165
LATS1	hsa-mir-16-5p, hsa-mir-335-5p	20371350, 18185580
LEF1	hsa-mir-34a-5p, hsa-mir-193b-3p	21566225|25587085|28098757, 20304954
LEFTY1	hsa-mir-302d-3p, hsa-mir-519c-3p, hsa-mir-519b-3p, hsa-mir-520d-3p, hsa-mir-519a-3p, hsa-mir-454-3p	21266536|22012620, 22012620, 22012620, 22012620, 22012620, 22012620
LEFTY2	hsa-mir-302d-3p	21266536
MACF1	hsa-mir-16-5p, hsa-mir-19a-3p, hsa-mir-19b-3p, hsa-mir-335-5p	18668040, 22473208, 22473208, 18185580
MBTD1	hsa-mir-149-5p	23622248
MEIS1	hsa-mir-484	23622248
MIXL1	hsa-mir-17-5p, hsa-mir-93-5p, hsa-mir-106a-5p, hsa-mir-302d-3p, hsa-mir-20b-5p, hsa-mir-519d-3p, hsa-mir-520d-3p, hsa-mir-520h	23446348, 23446348, 23446348, 23446348, 23446348, 23446348, 23446348, 23446348
MTF2	hsa-mir-19a-3p, hsa-mir-30c-5p	23622248, 20371350|27292025
NANOG	hsa-mir-34a-5p, hsa-mir-335-5p	22020437, 18185580
PBX3	hsa-mir-93-5p, hsa-mir-497-5p	20371350, 28042507
PHF6	hsa-mir-17-5p, hsa-mir-93-5p, hsa-mir-20b-5p, hsa-mir-519d-3p	22473208, 22473208, 22473208, 22473208
PITX2	hsa-mir-374b-5p	21572407
POU5F1	hsa-mir-34a-5p, hsa-mir-335-5p	24457968, 24859837|28239298
PPP2CA	hsa-mir-520c-5p, hsa-mir-518d-5p	23446348|21572407|20371350, 23446348|21572407|20371350

Target	Down-regulated microRNA	PMID
PRKAR1A	hsa-mir-16-5p, hsa-mir-17-5p, hsa-mir-93-5p, hsa-mir-106a-5p, hsa-mir-30c-5p, hsa-mir-20b-5p, hsa-mir-515-3p, hsa-mir-519e-3p, hsa-mir-519d-3p	18668040, 22012620, 22012620, 22012620, 23313552, 22012620, 22012620, 22012620, 22012620
RARG	hsa-mir-335-5p	18185580
SESN1	hsa-mir-17-5p, hsa-mir-93-5p, hsa-mir-106a-5p, hsa-mir-20b-5p, hsa-mir-519d-3p	27292025, 27292025, 27292025, 27292025, 27292025
SLC2A12	hsa-mir-335-5p	18185580
SMAD1	hsa-mir-16-5p, hsa-mir-30c-5p	18668040, 22253433
SOX17	hsa-mir-335-5p	24449834
SOX2	hsa-mir-34a-5p, hsa-mir-625-5p	22020437, 24508466
TBX1	hsa-mir-484	23622248
TCF4	hsa-mir-17-5p, hsa-mir-19b-3p, hsa-mir-93-5p, hsa-mir-20b-5p, hsa-mir-519d-3p	22473208, 20371350, 22473208, 22473208, 22473208
TEAD2	hsa-mir-335-5p, hsa-mir-193b-3p	18185580, 23622248
TET1	hsa-mir-454-3p	23622248
TOX3	hsa-mir-149-5p	23622248
TRERF1	hsa-mir-335-5p	18185580
TRIM71	hsa-mir-17-5p, hsa-mir-133a-3p, hsa-mir-133b, hsa-mir-454-3p	23622248, 23824327, 23824327, 22012620
TWSG1	hsa-mir-149-5p	23824327
UBR5	hsa-mir-17-5p, hsa-mir-93-5p, hsa-mir-20b-5p, hsa-mir-484, hsa-mir-519d-3p	22473208, 20371350|22473208, 22473208, 20371350, 22473208
WDFY2	hsa-mir-19b-3p, hsa-mir-30c-5p	22382630, 22473208
WNT3	hsa-mir-335-5p	18185580
WNT3A	hsa-mir-15a-5p, hsa-mir-16-5p	18931683|21106054, 18931683|20371350
ZIC2	hsa-mir-93-5p	23622248
ZIC5	hsa-mir-19a-3p, hsa-mir-19b-3p, hsa-mir-93-5p, hsa-mir-454-3p, hsa-mir-500a-5p, hsa-mir-556-3p	21572407, 21572407, 20371350, 21572407, 23446348|21572407|20371350, 21572407
ZNF281	hsa-mir-335-5p, hsa-mir-518f-3p, hsa-mir-518b, hsa-mir-518a-3p, hsa-mir-130a-5p	23592263|23824327, 20371350, 20371350, 20371350, 24398324|23446348|21572407

Appendix Table 4 : Table of miRs that target the 66 mRNAs in figure 5B

References

Bain, G., Kitchens, D., Yao, M., Huettner, J. E., & Gottlieb, D. I. (1995). Embryonic stem cells express neuronal properties in vitro. *Developmental Biology*, *168*(2), 342–357.

Bielby, R. C., Boccaccini, A. R., Polak, J. M., & Buttery, L. D. K. (2004). In vitro differentiation and in vivo mineralization of osteogenic cells derived from human embryonic stem cells. *Tissue Engineering*, *10*(9–10), 1518–1525.

Boyle, E. I., Weng, S., Gollub, J., Jin, H., Botstein, D., Cherry, J. M., & Sherlock, G. (2004). GO::TermFinder--open source software for accessing Gene Ontology information and finding significantly enriched Gene Ontology terms associated with a list of genes. *Bioinformatics (Oxford, England)*, *20*(18), 3710–3715.

Broughton, J. P., Lovci, M. T., Huang, J. L., Yeo, G. W., & Pasquinelli, A. E. (2016). Pairing beyond the seed supports MicroRNA targeting specificity. *Molecular Cell*, *64*(2), 320–333.

Brown, N. A., Holt, D., & Webb, M. (1984). The teratogenicity of methoxyacetic acid in the rat. *Toxicology Letters*, *22*(1), 93–100.

Buttery, L. D., Bourne, S., Xynos, J. D., Wood, H., Hughes, F. J., Hughes, S. P., Episkopou, V., & Polak, J. M. (2001). Differentiation of osteoblasts and in vitro bone formation from murine embryonic stem cells. *Tissue Engineering*, *7*(1), 89–99.

Capece, V., Garcia Vizcaino, J. C., Vidal, R., Rahman, R.-U., Pena Centeno, T., Shomroni, O., Suberviola, I., Fischer, A., & Bonn, S. (2015). Oasis: online analysis of small RNA deep sequencing data. *Bioinformatics (Oxford, England)*, *31*(13), 2205–2207.

Carroll, S. H., Macias Trevino, C., Li, E. B., Kawasaki, K., Myers, N., Hallett, S. A., Alhazmi, N., Cotney, J., Carstens, R. P., & Liao, E. C. (2020). An Irf6-Esrp1/2 regulatory axis controls midface morphogenesis in vertebrates. *Development (Cambridge, England)*, *147*(24), dev194498.

Cattane, N., Courtin, C., Mombelli, E., Maj, C., Mora, C., Etain, B., Bellivier, F., Marie-Claire, C., & Cattaneo, A. (2022). Transcriptomics and miRNomics data integration in lymphoblastoid cells highlights the key role of immune-related functions in lithium treatment response in Bipolar disorder. *BMC Psychiatry*, *22*(1). https://doi.org/10.1186/s12888-022-04286-3

Chang, L., & Xia, J. (2023). MicroRNA regulatory network analysis using miRNet 2.0. *Methods in Molecular Biology (Clifton, N.J.)*, *2594*, 185–204.

Chang, W., Cheng, J., Allaire, J., Sievert, C., Schloerke, B., Xie, Y., Allen, J., McPherson, J., Dipert, A., & Borges, B. (2022). *shiny: Web Application Framework for R* (1.7.2) [Computer software]. https://CRAN.R-project.org/package=shiny

Cheng, S. L., Yang, J. W., Rifas, L., Zhang, S. F., & Avioli, L. V. (1994). Differentiation of human bone marrow osteogenic stromal cells in vitro: induction of the osteoblast phenotype by dexamethasone. *Endocrinology*, *134*(1), 277–286.

Chentoufi, J., Hott, M., Lamblin, D., Buc-Caron, M. H., Marie, P. J., & Kellermann, O. (1993). Kinetics of in vitro mineralization by an osteogenic clonal cell line (C1) derived from mouse teratocarcinoma. *Differentiation; Research in Biological Diversity*, *53*(3), 181–189.

Chu, L.-F., Mamott, D., Ni, Z., Bacher, R., Liu, C., Swanson, S., Kendziorski, C., Stewart, R., & Thomson, J. A. (2019). An in vitro human segmentation clock model derived from embryonic stem cells. *Cell Reports*, *28*(9), 2247-2255.e5.

Dady, A., Blavet, C., & Duband, J.-L. (2012). Timing and kinetics of E- to N-cadherin switch during neurulation in the avian embryo. *Developmental Dynamics: An Official Publication of the American Association of Anatomists*, *241*(8), 1333–1349.

Dani, C., Smith, A. G., Dessolin, S., Leroy, P., Staccini, L., Villageois, P., Darimont, C., & Ailhaud, G. (1997). Differentiation of embryonic stem cells into adipocytes in vitro. *Journal of Cell Science*, *110 (Pt 11)*, 1279–1285.

de Leeuw, V. C., van Nieuwland, M., Bokkers, B. G. H., & Piersma, A. H. (2020). Culture conditions affect chemical-induced developmental toxicity in vitro: The case of folic acid, methionine and methotrexate in the neural embryonic stem cell test. *Alternatives to Laboratory Animals: ATLA*, *48*(4), 173–183.

Deichmann, C., Link, M., Seyfang, M., Knotz, V., Gradl, D., & Wedlich, D. (2015). Neural crest specification by Prohibitin1 depends on transcriptional regulation of prl3 and vangl1. *Genesis (New York, N.Y.: 2000)*, *53*(10), 627–639.

Du, Z.-W., Ma, L.-X., Phillips, C., & Zhang, S.-C. (2013). miR-200 and miR-96 families repress neural induction from human embryonic stem cells. *Development (Cambridge, England)*, *140*(12), 2611–2618.

Dunn, M. K., Mercola, M., & Moore, D. D. (1995). Cyclopamine, a steroidal alkaloid, disrupts development of cranial neural crest cells in Xenopus. *Developmental Dynamics: An Official Publication of the American Association of Anatomists*, *202*(3), 255–270.

Enomoto-Iwamoto, M., Kitagaki, J., Koyama, E., Tamamura, Y., Wu, C., Kanatani, N., Koike, T., Okada, H., Komori, T., Yoneda, T., Church, V., Francis-West, P. H., Kurisu, K., Nohno, T., Pacifici, M., & Iwamoto, M. (2002). The wnt antagonist frzb-1 regulates chondrocyte maturation and long bone development during limb skeletogenesis. *Developmental Biology*, *251*(1), 142–156.

Filipów, S., & Łaczmański, Ł. (2019). Blood circulating miRNAs as cancer biomarkers for diagnosis and surgical treatment response. *Frontiers in Genetics*, *10*, 169.

Focaccetti, C., Bruno, A., Magnani, E., Bartolini, D., Principi, E., Dallaglio, K., Bucci, E. O., Finzi, G., Sessa, F., Noonan, D. M., & Albini, A. (2015). Effects of 5-fluorouracil on morphology, cell cycle, proliferation, apoptosis, autophagy and ROS production in endothelial cells and cardiomyocytes. *PloS One*, *10*(2), e0115686.

Franceschi, R. T., & Iyer, B. S. (1992). Relationship between collagen synthesis and expression of the osteoblast phenotype in MC3T3-E1 cells. *Journal of Bone and Mineral Research: The Official Journal of the American Society for Bone and Mineral Research*, *7*(2), 235–246.

Friedländer, M. R., Mackowiak, S. D., Li, N., Chen, W., & Rajewsky, N. (2012). miRDeep2 accurately identifies known and hundreds of novel microRNA genes in seven animal clades. *Nucleic Acids Research*, *40*(1), 37–52.

Friedman, R. C., Farh, K. K.-H., Burge, C. B., & Bartel, D. P. (2009). Most mammalian mRNAs are conserved targets of microRNAs. *Genome Research*, *19*(1), 92–105.

Fukushima, T., Hamada, Y., Yamada, H., & Horii, I. (2007). Changes of micro-RNA expression in rat liver treated by acetaminophen or carbon tetrachloride--regulating role of micro-RNA for RNA expression. *The Journal of Toxicological Sciences*, *32*(4), 401–409.

Fuller, L. C., Cornelius, S. K., Murphy, C. W., & Wiens, D. J. (2002). Neural crest cell motility in valproic acid. *Reproductive Toxicology (Elmsford, N.Y.)*, *16*(6), 825–839.

Gasimli, L., Hickey, A. M., Yang, B., Li, G., dela Rosa, M., Nairn, A. V., Kulik, M. J., Dordick, J. S., Moremen, K. W., Dalton, S., & Linhardt, R. J. (2014). Changes in glycosaminoglycan structure on differentiation of human embryonic stem cells

towards mesoderm and endoderm lineages. *Biochimica et Biophysica Acta*, *1840*(6), 1993–2003.

Gebert, L. F. R., & MacRae, I. J. (2019). Regulation of microRNA function in animals. *Nature Reviews. Molecular Cell Biology*, *20*(1), 21–37.

George, R. M., Maldonado-Velez, G., & Firulli, A. B. (2020). The heart of the neural crest: cardiac neural crest cells in development and regeneration. *Development (Cambridge, England)*, *147*(20). https://doi.org/10.1242/dev.188706

Gessert, S., Bugner, V., Tecza, A., Pinker, M., & Kühl, M. (2010). FMR1/FXR1 and the miRNA pathway are required for eye and neural crest development. *Developmental Biology*, *341*(1), 222–235.

Ghafouri-Fard, S., Abak, A., Tondro Anamag, F., Shoorei, H., Fattahi, F., Javadinia, S. A., Basiri, A., & Taheri, M. (2021). 5-fluorouracil: A narrative review on the role of regulatory mechanisms in driving resistance to this chemotherapeutic agent. *Frontiers in Oncology*, *11*, 658636.

Ghassibe-Sabbagh, M., El Hajj, J., Al Saneh, M., El Baba, N., Abou Issa, J., Al Haddad, M., El Atat, O., Sabbagh, J., Abou Chebel, N., & El-Sibai, M. (2021). Altered regulation of cell migration in IRF6-mutated orofacial cleft patients-derived primary cells reveals a novel role of Rho GTPases in cleft/lip palate development. *Cells & Development*, *166*, 203674.

Gruneberg, H. (1958). Genetical studies on the skeleton of the mouse. XXIII. The development of brachyury and anury. *Journal of Embryology and Experimental Morphology*, *6*(3), 424–443.

Ha, M., & Kim, V. N. (2014). Regulation of microRNA biogenesis. *Nature Reviews. Molecular Cell Biology*, *15*(8), 509–524.

Hackenberg, M., Rodríguez-Ezpeleta, N., & Aransay, A. M. (2011). miRanalyzer: an update on the detection and analysis of microRNAs in high-throughput sequencing experiments. *Nucleic Acids Research*, *39*(Web Server issue), W132-8.

Hockman, D., Chong-Morrison, V., Green, S. A., Gavriouchkina, D., Candido-Ferreira, I., Ling, I. T. C., Williams, R. M., Amemiya, C. T., Smith, J. J., Bronner, M. E., & Sauka-Spengler, T. (2019). A genome-wide assessment of the ancestral neural crest gene regulatory network. *Nature Communications*, *10*(1), 4689.

Hyoun, S. C., Običan, S. G., & Scialli, A. R. (2012). Teratogen update: methotrexate. *Birth Defects Research. Part A, Clinical and Molecular Teratology*, *94*(4), 187–207.

Kang, S. W., Chae, H. Z., Seo, M. S., Kim, K., Baines, I. C., & Rhee, S. G. (1998). Mammalian peroxiredoxin isoforms can reduce hydrogen peroxide generated in response to growth factors and tumor necrosis factor-alpha. *The Journal of Biological Chemistry*, *273*(11), 6297–6302.

Katagiri, T., Yamaguchi, A., Ikeda, T., Yoshiki, S., Wozney, J. M., Rosen, V., Wang, E. A., Tanaka, H., Omura, S., & Suda, T. (1990). The non-osteogenic mouse pluripotent cell line, C3H10T1/2, is induced to differentiate into osteoblastic cells by recombinant human bone morphogenetic protein-2. *Biochemical and Biophysical Research Communications*, *172*(1), 295–299.

Kawaguchi, J., Mee, P. J., & Smith, A. G. (2005). Osteogenic and chondrogenic differentiation of embryonic stem cells in response to specific growth factors. *Bone*, *36*(5), 758–769.

Kim, Y.-K., & Kim, V. N. (2007). Processing of intronic microRNAs. *The EMBO Journal*, *26*(3), 775–783.

Komori, T., Yagi, H., Nomura, S., Yamaguchi, A., Sasaki, K., Deguchi, K., Shimizu, Y., Bronson, R. T., Gao, Y. H., Inada, M., Sato, M., Okamoto, R., Kitamura, Y., Yoshiki, S., & Kishimoto, T. (1997). Targeted disruption of Cbfa1 results in a complete lack of bone formation owing to maturational arrest of osteoblasts. *Cell*, *89*(5), 755–764.

Kozomara, A., Birgaoanu, M., & Griffiths-Jones, S. (2019). miRBase: from microRNA sequences to function. *Nucleic Acids Research*, *47*(D1), D155–D162.

Kozomara, A., & Griffiths-Jones, S. (2014). miRBase: annotating high confidence microRNAs using deep sequencing data. *Nucleic Acids Research*, *42*(Database issue), D68-73.

Kramer, J., Hegert, C., Guan, K., Wobus, A. M., Müller, P. K., & Rohwedel, J. (2000). Embryonic stem cell-derived chondrogenic differentiation in vitro: activation by BMP-2 and BMP-4. *Mechanisms of Development*, *92*(2), 193–205.

Kumar, V., Kumar, V., Chaudhary, A. K., Coulter, D. W., McGuire, T., & Mahato, R. I. (2018). Impact of miRNA-mRNA profiling and their correlation on medulloblastoma tumorigenesis. *Molecular Therapy. Nucleic Acids*, *12*, 490–503.

Kume, T., Jiang, H., Topczewska, J. M., & Hogan, B. L. (2001). The murine winged helix transcription factors, Foxc1 and Foxc2, are both required for cardiovascular development and somitogenesis. *Genes & Development*, *15*(18), 2470–2482.

Kunisada, T., Yoshida, H., Yamazaki, H., Miyamoto, A., Hemmi, H., Nishimura, E., Shultz, L. D., Nishikawa, S., & Hayashi, S. (1998). Transgene expression of steel factor in the basal layer of epidermis promotes survival, proliferation, differentiation and migration of melanocyte precursors. *Development (Cambridge, England)*, *125*(15), 2915–2923.

Kuske, B., Savkovic, V., & zur Nieden, N. I. (2011). Improved media compositions for the differentiation of embryonic stem cells into osteoblasts and chondrocytes. *Methods in Molecular Biology* , *690*, 195–215.

Le Douarin, N. M., & Teillet, M. A. (1973). The migration of neural crest cells to the wall of the digestive tract in avian embryo. *Journal of Embryology and Experimental Morphology*, *30*(1), 31–48.

Le Lièvre, C. S., & Le Douarin, N. M. (1975). Mesenchymal derivatives of the neural crest: analysis of chimaeric quail and chick embryos. *Journal of Embryology and Experimental Morphology*, *34*(1), 125–154.

Lee, J. E., & Lee, D. R. (2011). Human embryonic stem cells: derivation, maintenance and cryopreservation. *International Journal of Stem Cells*, *4*(1), 9–17.

Lee, R. C., Feinbaum, R. L., & Ambros, V. (1993). The C. elegans heterochronic gene lin-4 encodes small RNAs with antisense complementarity to lin-14. *Cell*, *75*(5), 843–854.

Lee, Y., Kim, M., Han, J., Yeom, K.-H., Lee, S., Baek, S. H., & Kim, V. N. (2004). MicroRNA genes are transcribed by RNA polymerase II. *The EMBO Journal*, *23*(20), 4051–4060.

Liao, J., Karnik, R., Gu, H., Ziller, M. J., Clement, K., Tsankov, A. M., Akopian, V., Gifford, C. A., Donaghey, J., Galonska, C., Pop, R., Reyon, D., Tsai, S. Q., Mallard, W., Joung, J. K., Rinn, J. L., Gnirke, A., & Meissner, A. (2015). Targeted disruption of DNMT1, DNMT3A and DNMT3B in human embryonic stem cells. *Nature Genetics*, *47*(5), 469–478.

Liu, X., Yu, J., Jiang, L., Wang, A., Shi, F., Ye, H., & Zhou, X. (2009). MicroRNA-222 regulates cell invasion by targeting matrix metalloproteinase 1 (MMP1) and manganese superoxide dismutase 2 (SOD2) in tongue squamous cell carcinoma cell lines. *Cancer Genomics & Proteomics*, *6*(3), 131–139.

Mackie, E. J., Ahmed, Y. A., Tatarczuch, L., Chen, K.-S., & Mirams, M. (2008). Endochondral ossification: how cartilage is converted into bone in the developing skeleton. *The International Journal of Biochemistry & Cell Biology*, *40*(1), 46–62.

Madrid, J. V., Sera, S. R., Sparks, N. R. L., & Zur Nieden, N. I. (2018). Human pluripotent stem cells to assess developmental toxicity in the osteogenic lineage. *Methods in Molecular Biology (Clifton, N.J.)*, *1797*, 125–145.

Mankoo, B. S., Skuntz, S., Harrigan, I., Grigorieva, E., Candia, A., Wright, C. V. E., Arnheiter, H., & Pachnis, V. (2003). The concerted action of Meox homeobox genes is required upstream of genetic pathways essential for the formation, patterning and differentiation of somites. *Development (Cambridge, England)*, *130*(19), 4655–4664.

Marsit, C. J., Eddy, K., & Kelsey, K. T. (2006). MicroRNA responses to cellular stress. *Cancer Research*, *66*(22), 10843–10848.

Matsuda, M., Yamanaka, Y., Uemura, M., Osawa, M., Saito, M. K., Nagahashi, A., Nishio, M., Guo, L., Ikegawa, S., Sakurai, S., Kihara, S., Maurissen, T. L., Nakamura, M., Matsumoto, T., Yoshitomi, H., Ikeya, M., Kawakami, N., Yamamoto, T., Woltjen, K., … Alev, C. (2020). Recapitulating the human segmentation clock with pluripotent stem cells. *Nature*, *580*(7801), 124–129.

Mavreli, D., Lykoudi, A., Lambrou, G., Papaioannou, G., Vrachnis, N., Kalantaridou, S., Papantoniou, N., & Kolialexi, A. (2020). Deep sequencing identified dysregulated circulating MicroRNAs in late onset preeclampsia. *In Vivo (Athens, Greece)*, *34*(5), 2317–2324.

McKinney, M. C., McLennan, R., Giniunaite, R., Baker, R. E., Maini, P. K., Othmer, H. G., & Kulesa, P. M. (2020). Visualizing mesoderm and neural crest cell dynamics during chick head morphogenesis. *Developmental Biology*, *461*(2), 184–196.

Meisig, J., Dreser, N., Kapitza, M., Henry, M., Rotshteyn, T., Rahnenführer, J., Hengstler, J. G., Sachinidis, A., Waldmann, T., Leist, M., & Blüthgen, N. (2020). Kinetic modeling of stem cell transcriptome dynamics to identify regulatory modules of normal and disturbed neuroectodermal differentiation. *Nucleic Acids Research*, *48*(22), 12577–12592.

Merrill, A. E., Bochukova, E. G., Brugger, S. M., Ishii, M., Pilz, D. T., Wall, S. A., Lyons, K. M., Wilkie, A. O. M., & Maxson, R. E., Jr. (2006). Cell mixing at a neural crest-mesoderm boundary and deficient ephrin-Eph signaling in the pathogenesis of craniosynostosis. *Human Molecular Genetics*, *15*(8), 1319–1328.

Mestdagh, P., Hartmann, N., Baeriswyl, L., Andreasen, D., Bernard, N., Chen, C., Cheo, D., D'Andrade, P., DeMayo, M., Dennis, L., Derveaux, S., Feng, Y., Fulmer-Smentek, S., Gerstmayer, B., Gouffon, J., Grimley, C., Lader, E., Lee, K. Y., Luo, S., … Vandesompele, J. (2014). Evaluation of quantitative miRNA expression

platforms in the microRNA quality control (miRQC) study. *Nature Methods*, *11*(8), 809–815.

Murabe, M., Yamauchi, J., Fujiwara, Y., Hiroyama, M., Sanbe, A., & Tanoue, A. (2007). A novel embryotoxic estimation method of VPA using ES cells differentiation system. *Biochemical and Biophysical Research Communications*, *352*(1), 164–169.

Nakajima, T., Shibata, M., Nishio, M., Nagata, S., Alev, C., Sakurai, H., Toguchida, J., & Ikeya, M. (2018). Modeling human somite development and fibrodysplasia ossificans progressiva with induced pluripotent stem cells. *Development (Cambridge, England)*, *145*(16). https://doi.org/10.1242/dev.165431

Nakashima, K., & de Crombrugghe, B. (2003). Transcriptional mechanisms in osteoblast differentiation and bone formation. *Trends in Genetics: TIG*, *19*(8), 458–466.

Nakashima, K., Zhou, X., Kunkel, G., Zhang, Z., Deng, J. M., Behringer, R. R., & de Crombrugghe, B. (2002). The novel zinc finger-containing transcription factor osterix is required for osteoblast differentiation and bone formation. *Cell*, *108*(1), 17–29.

Nersisyan, S., Shkurnikov, M., Turchinovich, A., Knyazev, E., & Tonevitsky, A. (2020). Integrative analysis of miRNA and mRNA sequencing data reveals potential regulatory mechanisms of ACE2 and TMPRSS2. *PloS One*, *15*(7), e0235987.

Otto, F., Thornell, A. P., Crompton, T., Denzel, A., Gilmour, K. C., Rosewell, I. R., Stamp, G. W., Beddington, R. S., Mundlos, S., Olsen, B. R., Selby, P. B., & Owen, M. J. (1997). Cbfa1, a candidate gene for cleidocranial dysplasia syndrome, is essential for osteoblast differentiation and bone development. *Cell*, *89*(5), 765–771.

Pasini, D., Cloos, P. A. C., Walfridsson, J., Olsson, L., Bukowski, J.-P., Johansen, J. V., Bak, M., Tommerup, N., Rappsilber, J., & Helin, K. (2010). JARID2 regulates binding of the Polycomb repressive complex 2 to target genes in ES cells. *Nature*, *464*(7286), 306–310.

Pasquinelli, A. E., Reinhart, B. J., Slack, F., Martindale, M. Q., Kuroda, M. I., Maller, B., Hayward, D. C., Ball, E. E., Degnan, B., Müller, P., Spring, J., Srinivasan, A., Fishman, M., Finnerty, J., Corbo, J., Levine, M., Leahy, P., Davidson, E., & Ruvkun, G. (2000). Conservation of the sequence and temporal expression of let-7 heterochronic regulatory RNA. *Nature*, *408*(6808), 86–89.

Patel, K., Chandrasegaran, S., Clark, I. M., Proctor, C. J., Young, D. A., & Shanley, D. P. (2021). TimiRGeN: R/Bioconductor package for time series microRNA-mRNA integration and analysis. *Bioinformatics (Oxford, England)*, *37*(20), 3604–3609.

Pekkinen, M., Terhal, P. A., Botto, L. D., Henning, P., Mäkitie, R. E., Roschger, P., Jain, A., Kol, M., Kjellberg, M. A., Paschalis, E. P., van Gassen, K., Murray, M., Bayrak-Toydemir, P., Magnusson, M. K., Jans, J., Kausar, M., Carey, J. C., Somerharju, P., Lerner, U. H., … Mäkitie, O. (2019). Osteoporosis and skeletal dysplasia caused by pathogenic variants in SGMS2. *JCI Insight*, *4*(7). https://doi.org/10.1172/jci.insight.126180

Phillips, B. W., Belmonte, N., Vernochet, C., Ailhaud, G., & Dani, C. (2001). Compactin enhances osteogenesis in murine embryonic stem cells. *Biochemical and Biophysical Research Communications*, *284*(2), 478–484.

Piacentino, M. L., Li, Y., & Bronner, M. E. (2020). Epithelial-to-mesenchymal transition and different migration strategies as viewed from the neural crest. *Current Opinion in Cell Biology*, *66*, 43–50.

Pogribny, I. P., Tryndyak, V. P., Boyko, A., Rodriguez-Juarez, R., Beland, F. A., & Kovalchuk, O. (2007). Induction of microRNAome deregulation in rat liver by long-term tamoxifen exposure. *Mutation Research*, *619*(1–2), 30–37.

Poliard, A., Nifuji, A., Lamblin, D., Plee, E., Forest, C., & Kellermann, O. (1995). Controlled conversion of an immortalized mesodermal progenitor cell towards osteogenic, chondrogenic, or adipogenic pathways. *The Journal of Cell Biology*, *130*(6), 1461–1472.

Pourquié, O., Fan, C. M., Coltey, M., Hirsinger, E., Watanabe, Y., Bréant, C., Francis-West, P., Brickell, P., Tessier-Lavigne, M., & Le Douarin, N. M. (1996). Lateral and axial signals involved in avian somite patterning: a role for BMP4. *Cell*, *84*(3), 461–471.

Pryor, S. E., Massa, V., Savery, D., Andre, P., Yang, Y., Greene, N. D. E., & Copp, A. J. (2014). Vangl-dependent planar cell polarity signalling is not required for neural crest migration in mammals. *Development (Cambridge, England)*, *141*(16), 3153–3158.

Ramchandran, R., & Chaluvally-Raghavan, P. (2017). MiRNA-mediated RNA activation in mammalian cells. *Advances in Experimental Medicine and Biology*, *983*, 81–89.

Rinaldi, L., Datta, D., Serrat, J., Morey, L., Solanas, G., Avgustinova, A., Blanco, E., Pons, J. I., Matallanas, D., Von Kriegsheim, A., Di Croce, L., & Benitah, S. A.

(2016). Dnmt3a and Dnmt3b associate with enhancers to regulate human epidermal stem cell homeostasis. *Cell Stem Cell, 19*(4), 491–501.

Rogers, C. D., Sorrells, L. K., & Bronner, M. E. (2018). A catenin-dependent balance between N-cadherin and E-cadherin controls neuroectodermal cell fate choices. *Mechanisms of Development*, *152*, 44–56.

Rohwedel, J., Maltsev, V., Bober, E., Arnold, H. H., Hescheler, J., & Wobus, A. M. (1994). Muscle cell differentiation of embryonic stem cells reflects myogenesis in vivo: developmentally regulated expression of myogenic determination genes and functional expression of ionic currents. *Developmental Biology*, *164*(1), 87–101.

Rosa, A., Papaioannou, M. D., Krzyspiak, J. E., & Brivanlou, A. H. (2014). miR-373 is regulated by TGFβ signaling and promotes mesendoderm differentiation in human Embryonic Stem Cells. *Developmental Biology*, *391*(1), 81–88.

Rueda, A., Barturen, G., Lebrón, R., Gómez-Martín, C., Alganza, Á., Oliver, J. L., & Hackenberg, M. (2015). sRNAtoolbox: an integrated collection of small RNA research tools. *Nucleic Acids Research*, *43*(W1), W467-73.

Saga, Y., Hata, N., Koseki, H., & Taketo, M. M. (1997). Mesp2: a novel mouse gene expressed in the presegmented mesoderm and essential for segmentation initiation. *Genes & Development*, *11*(14), 1827–1839.

Sahakyan, V., Pozzo, E., Duelen, R., Deprest, J., & Sampaolesi, M. (2017). Methotrexate and valproic acid affect early neurogenesis of human amniotic fluid stem cells from myelomeningocele. *Stem Cells International*, *2017*, 1–10.

Sathyan, P., Golden, H. B., & Miranda, R. C. (2007). Competing interactions between micro-RNAs determine neural progenitor survival and proliferation after ethanol exposure: evidence from an ex vivo model of the fetal cerebral cortical neuroepithelium. *The Journal of Neuroscience: The Official Journal of the Society for Neuroscience*, *27*(32), 8546–8557.

Schlicker, C., Gertz, M., Papatheodorou, P., Kachholz, B., Becker, C. F. W., & Steegborn, C. (2008). Substrates and regulation mechanisms for the human mitochondrial sirtuins Sirt3 and Sirt5. *Journal of Molecular Biology*, *382*(3), 790–801.

Scholz, G., Genschow, E., Pohl, I., Bremer, S., Paparella, M., Raabe, H., Southee, J., & Spielmann, H. (1999). Prevalidation of the Embryonic Stem Cell Test (EST)-A new in vitro embryotoxicity test. *Toxicology in Vitro: An International Journal Published in Association with BIBRA*, *13*(4–5), 675–681.

Schraml, E., Hackl, M., & Grillari, J. (2017). MicroRNAs and toxicology: A love marriage. *Toxicology Reports*, *4*, 634–636.

Schriml, L. M., Arze, C., Nadendla, S., Chang, Y.-W. W., Mazaitis, M., Felix, V., Feng, G., & Kibbe, W. A. (2012). Disease Ontology: a backbone for disease semantic integration. *Nucleic Acids Research*, *40*(Database issue), D940-6.

Sera, S. R., & Zur Nieden, N. I. (2017). microRNA Regulation of Skeletal Development. *Current Osteoporosis Reports*, *15*(4), 353–366.

Setten, R. L., Rossi, J. J., & Han, S.-P. (2019). The current state and future directions of RNAi-based therapeutics. *Nature Reviews. Drug Discovery*, *18*(6), 421–446.

Simões-Costa, M., & Bronner, M. E. (2015). Establishing neural crest identity: a gene regulatory recipe. *Development* , *142*(2), 242–257.

Sparks, N. R. L., Martinez, I. K. C., Soto, C. H., & Zur Nieden, N. I. (2018). Low Osteogenic Yield in Human Pluripotent Stem Cells Associates with Differential Neural Crest Promoter Methylation. *Stem Cells*, *36*(3), 349–362.

Spielmann, H., Pohl, I., Döring, B., Liebsch, M., & Moldenhauer, F. (1998). The embryonic stem cell test (EST), an in vitro embryotoxicity test using two permanent mouse cell lines: 3T3 fibroblasts and embryonic stem cells. In *Ersatz- und Ergänzungsmethoden zu Tierversuchen* (pp. 289–290). Springer Vienna.

Stepniak, E., Radice, G. L., & Vasioukhin, V. (2009). Adhesive and signaling functions of cadherins and catenins in vertebrate development. *Cold Spring Harbor Perspectives in Biology*, *1*(5), a002949.

Strimbu, K., & Tavel, J. A. (2010). What are biomarkers? *Current Opinion in HIV and AIDS*, *5*(6), 463–466.

Tagliaferri, S., Cepparulo, P., Vinciguerra, A., Campanile, M., Esposito, G., Maruotti, G. M., Zullo, F., Annunziato, L., & Pignataro, G. (2021). MiR-16-5p, miR-103-3p, and miR-27b-3p as early peripheral biomarkers of fetal growth restriction. *Frontiers in Pediatrics*, *9*, 611112.

Takarada, T., Nakazato, R., Tsuchikane, A., Fujikawa, K., Iezaki, T., Yoneda, Y., & Hinoi, E. (2016). Genetic analysis of Runx2 function during intramembranous ossification. *Development (Cambridge, England)*, *143*(2), 211–218.

Takemoto, T., Uchikawa, M., Yoshida, M., Bell, D. M., Lovell-Badge, R., Papaioannou, V. E., & Kondoh, H. (2011). Tbx6-dependent Sox2 regulation determines neural or mesodermal fate in axial stem cells. *Nature*, *470*(7334), 394–398.

Tonegawa, A., & Takahashi, Y. (1998). Somitogenesis controlled by Noggin. *Developmental Biology*, *202*(2), 172–182.

Tribolet, L., Kerr, E., Cowled, C., Bean, A. G. D., Stewart, C. R., Dearnley, M., & Farr, R. J. (2020). MicroRNA biomarkers for infectious diseases: From basic research to biosensing. *Frontiers in Microbiology*, *11*, 1197.

Vasudevan, S. (2012). Posttranscriptional upregulation by microRNAs. *Wiley Interdisciplinary Reviews. RNA*, *3*(3), 311–330.

Vaux, K. K., Kahole, N. C. O., & Jones, K. L. (2003). Cyclophosphamide, methotrexate, and cytarabine embropathy: is apoptosis the common pathway? *Birth Defects Research. Part A, Clinical and Molecular Teratology*, *67*(6), 403–408.

Walker, L., Baumgartner, L., Keller, K. C., Ast, J., Trettner, S., & Zur Nieden, N. I. (2014). Non-human primate and rodent embryonic stem cells are differentially sensitive to embryotoxic compounds. *Toxicology Reports*, *2*, 165–174.

Wang, L., Zhu, J., Deng, F.-Y., Wu, L.-F., Mo, X.-B., Zhu, X.-W., Xia, W., Xie, F.-F., He, P., Bing, P.-F., Qiu, Y.-H., Lin, X., Lu, X., Zhang, L., Yi, N.-J., Zhang, Y.-H., & Lei, S.-F. (2018). Correlation analyses revealed global microRNA–mRNA expression associations in human peripheral blood mononuclear cells. *Molecular Genetics and Genomics: MGG*, *293*(1), 95–105.

Wang, M., Marco, P. de, Capra, V., & Kibar, Z. (2019). Update on the role of the non-canonical Wnt/planar cell polarity pathway in neural tube defects. *Cells (Basel, Switzerland)*, *8*(10), 1198.

Wang, T.-T., Lee, C.-Y., Lai, L.-C., Tsai, M.-H., Lu, T.-P., & Chuang, E. Y. (2019). anamiR: integrated analysis of MicroRNA and gene expression profiling. *BMC Bioinformatics*, *20*(1). https://doi.org/10.1186/s12859-019-2870-x

Weber, J. A., Baxter, D. H., Zhang, S., Huang, D. Y., Huang, K. H., Lee, M. J., Galas, D. J., & Wang, K. (2010). The microRNA spectrum in 12 body fluids. *Clinical Chemistry*, *56*(11), 1733–1741.

Weiner, A. M. J. (2018). MicroRNAs and the neural crest: From induction to differentiation. *Mechanisms of Development*, *154*, 98–106.

Wightman, B., Ha, I., & Ruvkun, G. (1993). Posttranscriptional regulation of the heterochronic gene lin-14 by lin-4 mediates temporal pattern formation in C. elegans. *Cell*, *75*(5), 855–862.

Williams, R. M., Lukoseviciute, M., Sauka-Spengler, T., & Bronner, M. E. (2022). Single-cell atlas of early chick development reveals gradual segregation of neural crest lineage from the neural plate border during neurulation. *ELife*, *11*. https://doi.org/10.7554/eLife.74464

Wong, R. K. Y., MacMahon, M., Woodside, J. V., & Simpson, D. A. (2019). A comparison of RNA extraction and sequencing protocols for detection of small RNAs in plasma. *BMC Genomics*, *20*(1), 446.

Xi, H., Fujiwara, W., Gonzalez, K., Jan, M., Liebscher, S., Van Handel, B., Schenke-Layland, K., & Pyle, A. D. (2017). In vivo human somitogenesis guides somite development from hPSCs. *Cell Reports*, *18*(6), 1573–1585.

Xi, J., Wu, Y., Li, G., Ma, L., Feng, K., Guo, X., Jia, W., Wang, G., Yang, G., Li, P., & Kang, J. (2017). Mir-29b mediates the neural tube versus neural crest fate decision during embryonic stem cell neural differentiation. *Stem Cell Reports*, *9*(2), 571–586.

Xu, Y., Fang, F., Zhang, J., Josson, S., St Clair, W. H., & St Clair, D. K. (2010). miR-17* suppresses tumorigenicity of prostate cancer by inhibiting mitochondrial antioxidant enzymes. *PloS One*, *5*(12), e14356.

Yagi, H., Takahata, Y., Murakami, T., Nakaminami, Y., Hagino, H., Yamamoto, S., Murakami, S., Hata, K., & Nishimura, R. (2022). Transcriptional regulation of FRZB in chondrocytes by Osterix and Msx2. *Journal of Bone and Mineral Metabolism*, *40*(5), 723–734.

Yamada, S., Yamazaki, D., & Kanda, Y. (2018). 5-Fluorouracil inhibits neural differentiation via Mfn1/2 reduction in human induced pluripotent stem cells. *The Journal of Toxicological Sciences*, *43*(12), 727–734.

Yanagisawa, T., Ouchi, T., Shibata, S., Negishi, T., & Okano, H. (2022). Glycosaminoglycans promote osteogenesis from human induced pluripotent stem cells via neural crest induction. *Biochemical and Biophysical Research Communications*, *603*, 49–56.

Yao, Y., Jiang, C., Wang, F., Yan, H., Long, D., Zhao, J., Wang, J., Zhang, C., Li, Y., Tian, X., Wang, Q. K., Wu, G., & Zhang, Z. (2019). Integrative analysis of miRNA and mRNA expression profiles associated with human atrial aging. *Frontiers in Physiology*, *10*, 1226.

Yoffe, L., Gilam, A., Yaron, O., Polsky, A., Farberov, L., Syngelaki, A., Nicolaides, K., Hod, M., & Shomron, N. (2018). Early detection of preeclampsia using

circulating small non-coding RNA. *Scientific Reports*, *8*(1). https://doi.org/10.1038/s41598-018-21604-6

Yoon, J. K., & Wold, B. (2000). The bHLH regulator pMesogenin1 is required for maturation and segmentation of paraxial mesoderm. *Genes & Development*, *14*(24), 3204–3214.

Yu, Y., Deng, P., Yu, B., Szymanski, J. M., Aghaloo, T., Hong, C., & Wang, C.-Y. (2017). Inhibition of EZH2 promotes human embryonic stem cell differentiation into mesoderm by reducing H3K27me3. *Stem Cell Reports*, *9*(3), 752–761.

Yuan, Z., Sun, X., Jiang, D., Ding, Y., Lu, Z., Gong, L., Liu, H., & Xie, J. (2010). Origin and evolution of a placental-specific microRNA family in the human genome. *BMC Evolutionary Biology*, *10*(1), 346.

Zhang, C., Cho, K., Huang, Y., Lyons, J. P., Zhou, X., Sinha, K., McCrea, P. D., & de Crombrugghe, B. (2008). Inhibition of Wnt signaling by the osteoblast-specific transcription factor Osterix. *Proceedings of the National Academy of Sciences of the United States of America*, *105*(19), 6936–6941.

Zhang, L., Wu, H., Zhao, M., Chang, C., & Lu, Q. (2020). Clinical significance of miRNAs in autoimmunity. *Journal of Autoimmunity*, *109*(102438), 102438.

Zhao, J., Li, S., Trilok, S., Tanaka, M., Jokubaitis-Jameson, V., Wang, B., Niwa, H., & Nakayama, N. (2014). Small molecule-directed specification of sclerotome-like chondroprogenitors and induction of a somitic chondrogenesis program from embryonic stem cells. *Development (Cambridge, England)*, *141*(20), 3848–3858.

Zhu, M.-X., Zhao, J.-Y., Chen, G.-A., & Guan, L. (2011). Early embryonic sensitivity to cyclophosphamide in cardiac differentiation from human embryonic stem cells. *Cell Biology International*, *35*(9), 927–938.

Ziemann, M., Kaspi, A., & El-Osta, A. (2016). Evaluation of microRNA alignment techniques. *RNA* , *22*(8), 1120–1138.

Zimmer, B., Lee, G., Balmer, N. V., Meganathan, K., Sachinidis, A., Studer, L., & Leist, M. (2012). Evaluation of developmental toxicants and signaling pathways in a functional test based on the migration of human neural crest cells. *Environmental Health Perspectives*, *120*(8), 1116–1122.

zur Nieden, N. I., & Baumgartner, L. (2010). Assessing developmental osteotoxicity of chlorides in the embryonic stem cell test. *Reproductive Toxicology (Elmsford, N.Y.)*, *30*(2), 277–283.

zur Nieden, N. I., Kempka, G., & Ahr, H. J. (2003). In vitro differentiation of embryonic stem cells into mineralized osteoblasts. *Differentiation; Research in Biological Diversity*, *71*(1), 18–27.

zur Nieden, N. I., Kempka, G., & Ahr, H. J. (2004). Molecular multiple endpoint embryonic stem cell test--a possible approach to test for the teratogenic potential of compounds. *Toxicology and Applied Pharmacology*, *194*(3), 257–269.